EFFECT OF COLUMN-BEAM MOMENT CAPACITY RATIOS ON THE FRAME PLASTIC FAILURE MECHANISM

A Thesis Submitted to
The Graduate School of Engineering and Sciences of
İzmir Institute of Technology
in partial Fulfillment of the Requirements for the Degree of

MASTER OF SCIENCE

In Civil Engineering

by
Rohullah AKHTARI

March 2023
İZMİR

ACKNOWLEDGEMENTS

First of all, I would like to thank my esteemed advisor Prof. Dr. Cemalettin Dönmez, for being an excellent mentor. This research would not have been possible without his support and guidance.

My gratitude extends to the civil engineering department for trusting me and providing me with the facility and the opportunity throughout my study.

I also thank the members of the jury Assoc. Prof. Engin Aktaş and Prof. Dr. Oğuz Özgür Eğilmez for offering comments and their precious time.

I express my sincerest gratitude to my mother, my sister, and my brothers for the unconditional encouragement and support that I needed throughout this process.

To my friends, this would have been a hard feat without you. Thank you for your unwavering support.

ABSTRACT

EFFECT OF COLUMN-BEAM MOMENT CAPACITY RATIOS ON THE FRAME PLASTIC FAILURE MECHANISM

The strong-column weak-beam design ratio plays a crucial rule to design the structures particularly for high seismic region. Interestingly, the ratio to be used is still under spotlight for research. Observations and analytical studies have demonstrated that the ratio's effectiveness varies with some parameters. One of these parameters is the number of stories in a building. The failure mechanism of the structures depends on this ratio and the design ratio efficiency seems to change as building's stories increases. This efficiency also seem to saturate at a point depending on number of stories.

In this study, three case studies have been assessed and analyzed. Each case study contains three reinforced concrete frames with different strong-column weak-beam design ratios that varies from 1.2 to 3.0. For each case study, the design ratios are ranged into three parts: (i) ratios between 1.2 to 1.5; (ii) ratios between 1.5 to 2.0; (iii) ratios between 2.0 to 3.0. The Turkish Earthquake Regulation (2018) has been utilized for the design procedures. The pushover and time-history analysis of frames were performed using OpenSees software framework (McKenna et al., 2010). Columns have been modeled with fiber sections and the beams have been modeled with concentrated rotational springs at the ends. Both members are accepted to be linear in between. The plastic hinge occurrence at the end of members were monitored to observe the frames' failure mechanism.

Keywords*: Strong-Column Weak-Beam; Column-Beam Moment Strength Ratio; Seismic Design; Plastic Hinges; Failure Mechanism.*

ÖZET

KOLON-KİRİŞ MOMENT KAPASİTE ORANLARININ ÇERÇEVE PLASTİK HASAR MEKANİZMASINA ETKİSİ

Güçlü kolon zayıf kiriş tasarım oranı, özellikle yüksek sismik bölgelerdeki yapıların tasarlanmasında çok önemli bir rol oynamasına rağmen kullanılacak değerin büyüklüğü araştırmacılar için hala bir araştırma konusudur. Gözlemler ve analitik çalışmalar, oranın göçme mekanizmasına etkisinin bazı değişkenlerden etkilendiğini göstermiştir. Bu değişkenlerden biri de binaların kat sayısıdır. Yapıların göçme mekanizma şeklinin bu orandan etkilendiği görülmekte ve bina kat sayısı arttıkça kulanılan tasarım oranının veriminin de değiştiği gözlenmektedir. Katsayıdaki artışa bağlı iyileşmenin kat sayısına bağlı olarak bir noktada doyuma ulaştığı ayrıca gözlenmektedir.

Bu tez kapsamında üç tip çerçeve tasarlanmış ve değerlendirilmiştir. Her çerçeve, 1.2 ila 3.0 arasında değişen farklı güçlü-kolon zayıf-kiriş tasarım oranlarına sahip üç tip çerçeve içermektedir. Her tip için tasarım oranları (i) 1.2 ile 15, (ii) 1.5 ila 2.0, (iii) 2.0 ila 3.0 değerlerine sahiptir. Çerçeve tasarımları Türk Deprem Yönetmeliğine (2018) uygun gerçekleştirilmiştir. Çerçevelerin itme ve zaman tanım alanında analizleri, OpenSees (McKenna et al., 2010) yazılım çerçevesi kullanılarak gerçekleştirilmiştir. Elemanların doğrusal olmayan davranışı kolonlarda eleman uçlarında fiber kesitler, kirişler de ise yine eleman uçlarındaki doğrusal olmayan eğilme yayları ile modellenmiştir. Her iki elemanda yaylar rasındaki bölgede elastik kabul edilmiştir. Çerçevelerin göçme mekanizmaları elemanların uçlarındaki plastik mafsal oluşumları izlenerek tanımlanmıştır.

***Anahtar Kelimeler**: Kuvvetli Kolon Zayıf kiriş; Kolon-Kiriş Moment Kapasitesi Oranı; Sismik Tasarım; Plastik Menteşeler; Başarısızlık Mekanizması.*

To my father

TABLE OF CONTENTS

LIST OF FIGURES

Figure **Page**

Figure **Page**

Figure **Page**

LIST OF TABLES

Table **Page**

Table **Page**

CHAPTER 1

INTRODUCTION

1.1 Background

Structural engineers developed many strategies to design buildings against the demands imposed by earthquakes. A widespread adopted methodology in the last half century is designing a system that is proportioned to fail in flexural mode. Moment frames are employed for this purpose. The source of such a strategy is the observation of the similar displacement demands for the same structure regardless it behaves in linear or nonlinear mode as long as initial stiffness are same. Due to the cost issues to design a system in the linear range, profession targeted for nonlinear response.

The approach is organized to have systems that develop sustainable and distributed displacements in the nonlinear range. Sustainability is achieved ensuring ductile flexure failures at the element level. Since the local concentration of the displacement demands could cause early capacity over limits, it is also needed to distribute the displacement through the frames. This requirement is attempted to ensure by proportioning to have a failure mode in a beam mechanism.

If a frame is not proportioned and detailed accordingly, local concentration of displacements could lead to story mechanism as shown in Figure 1. If such a mechanism developed the plastic flexural capacities of the members exhausted at early roof drift levels. Alternative mechanism is formation of hinges all through the structure at beam ends as shown Figure 2. Here, contributions from each story to roof drift ratio cause a decrease of demands from individual members.

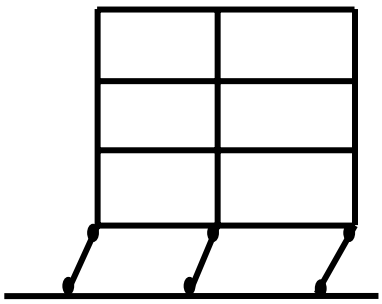

Figure 1. Story mechanism failure

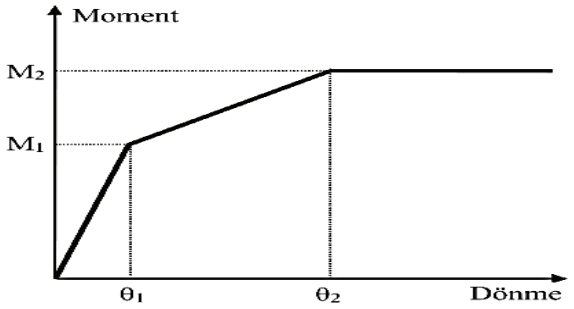

Figure 2. Capacity or pushover curve (TSC, 2018)

Seismic regulations (Turkish Seismic Code 2018, ASCE 7-16) attempted to enforce the beam mechanism formation through control of the total column moment capacity to total moment capacity at a beam-column joint. A limit ratio of 1.2 is generally accepted (Turkish Seismic Code 2018). The accepted moment layout that leads to calculation of ratios is shown Figure 3. It is known that the defined requirement is solely not sufficient to ensure the beam mechanism. Studies show that some other parameters can also effect the failure mechanism.

1.2 Literature Review

A study conducted by Haselton and Deierlein (2007) show the importance of three design parameters (design base shear strength, design interstory drift limit, and strong-column weak-beam design ratio) that affect collapse safety. This study worked on frames ranging from 4 to 12 stories. A nonlinear model was created for each building along with collapse simulations. Based on the findings of this study, the strong-column weak-beam (SCWB) design ratio is the most vital parameter among the others. The results of this study show that collapse performance was improved as the SCWB design ratio was increased and it guided the system to contain full collapse mechanism. For 12-story buildings, SCWB design ratio up to 3.0 can improve the collapse capacity due to improving the collapsing mechanism.

However, it was seen that beyond SCWB design ratio of 1.5, no further improvement in the mechanism occurs for 4-story buildings. Study only concentrated on the defined three parameters mentioned above and did not consider the effects of element detailing requirement.

Another study done by Zareian,F (2006) investigated the effect of column to beam strength ratio on moment-resisting frames. Two case study structures are considered. Structures were thoroughly addressed about the collapse fragility curve characteristics - namely, the median of collapse capacity reacted to changes in the structural parameters. It is concluded that the ratio of columns to beam strength (CBS) alongside P-Delta are the main important parameters that impact the collapse potential. It was shown that raising the CBS from 1.2 to 2.4 results in a 90% increase in the median collapse capacity. The stiffness of structural parts, particularly the stiffness of the columns in the lower levels of the building, is reported to be decreased by P-Delta. This result causes a story mechanism to evolve in the structure's bottom regions. Study showed that this phenomenon can be delayed and nonlinear behavior can be concentrated more into the beams by increasing column strength.

The effect of the column-to-beam strength ratio was investigated for steel moment frames under seismic response by Zaghi et al., 2014. Various parameters such as floor acceleration, inter-story drift, and member ductility were taken into consideration. For every frame, the column section sizes and yield strength of material varied until reaching desired column beam strength ratios. It was found that the maximum story drifts and yield base shear are independent of the column-beam strength ratio. However, they were somehow related to beam strength. The effects of higher modes on columns' yield strength were monitored and it was shown that these effects can cause columns to yield even for a strength ratio of larger than 2.

A study carried out by Sudarsana (2014) demonstrates the column-to-beam strength ratio impacts the behavior of ductile reinforced concrete frames under static nonlinear pushover analysis. The main parameter of this study is the column-to-beam strength ratio ranging from 1.2 up to 2.0 using the nominal strength of columns and beams. It was found that a strength ratio of up to 1.4 can improve ductility. However, beyond this ratio for five and ten- story models, the improvement in ductility is not seen. For strength ratios of 1.4 up to 2.0, a beam sway collapse mechanism was attained for five-story frames, and for ten-story frame models, this value changes from 1.6 to 2.0.

Caterino et al. (2013) proposed a method to calculate the lateral stiffness and inter-story drift ratio of frames considering their relation. An approximate method which was conducted on 9 'ideal' and 2 'real frames is assessed based on the Italian Seismic Code. The results were then compared to other studies showing a better approximation of

parameters for those buildings in which ‘capacity design’ were used. The analysis was based on the first vibration mode shape for the estimation of inter-story drift and stiffness. The authors first calculated the stiffness and then assessed the inter-story drift based on the suggested formula. The results were a better approximation for shear-type framing compared to flexure type in this study.

Hao Zhang et al. (2019) studied the impact of column-to-beam strength on failure modes for a reinforced concrete frame. The strength ratios varied from 1.2 up to 2.0, and a pushover analysis was conducted to figure out the behavior of the system. In this study, it is proposed to increase the column-to-beam ratio. Analysis was performed on a 3-story 3-bay frame that was designed according to China’s seismic design code. Furthermore, it was shown that in order to achieve the strong column and weak beam failure mode, the strength ratio should increase up to 1.8 considering the effects of slabs.

An optimal seismic method was proposed by Choi et al. (2014) to induce the beam-hinging mechanism. This method was applied to a four-story reinforced concrete moment frame in order to verify it. The mentioned method consists of three constraints, avoiding the plastic hinge of columns, the column-to-beam strength ratio, and the strength of columns and beams. To evaluate the energy dissipation capacity of the system and plastic hinge constraints, a nonlinear static analysis is employed. An optimization tool which is called non-dominated genetic algorithm II was utilized in this method together with a multi-core-based parallel assessment to accelerate the process.

Another study was conducted by Nakashima M, and Sawaizumi S (2000) which describes the required column-to-beam strength ratio in steel moment frames. In this study, the column overstrength factor (COF9 in comply with the AISC Seismic Provisions (1997), is defined as the ratio of column plastic moment capacity to beam plastic moment capacity (taking into account the existence of axial loads). It was shown that the magnitude of the column over strength required for this mechanism increases as ground motion amplitude increases and it ranges between 1.5 to 2. Study also demonstrated that as ground motion amplitude raised, the maximum story drift relative to the maximum overall drift also increases.

Turkish Seismic code (2018) defines the way of calculating the column-to-beam strength ratios as it is shown in equation (1.1) and figure 3.

$$(M_{ra} + M_{rü}) \geq 1.2\,(M_{ri} + M_{rj}) \tag{1.1}$$

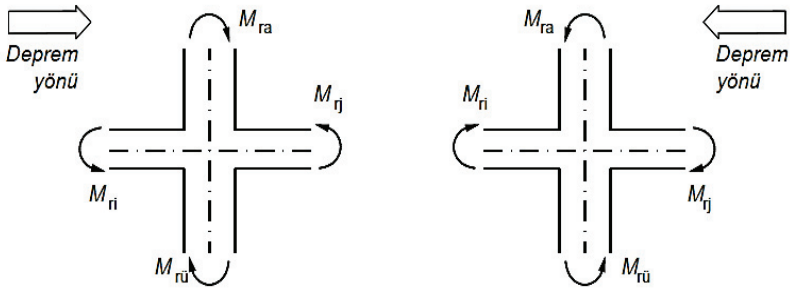

Figure 3. Representation of moments in strong-column weak-beams (TSC, 2018)

1.3 Objective and Scope of the Study

The main goal of this study is to observe the failure mechanisms of RC moment frames that satisfies the Turkish Earthquake Regulation (TER 2018). Two, five, and eight-story RC frames are selected to reference the existing low height RC structures in Turkey. Selected structures are two-dimensional three-bays frames which are designed to satisfy the industry typical span lengths and mass distributions. Stiffness along the height are well distributed. Several column-to-beam flexural strength ratios were applied to see the response of the frames. The design requirements per TS500 and TSC 2018 is satisfied. Each frame is analyzed with column-beam strength ratios ranging from 1.2 to 4.

Static nonlinear analysis (pushover) and nonlinear time history analysis are carried out to observe the frame failure mechanism. These analyses are conducted using OpenSees software framework (McKenna et al., 2010). Columns are discretized with fiber sections and the beams with concentrated plastic hinges at their ends. Rest of the both columns and beams are considered elastic. The members' deformations were assumed to be only under flexural actions. It is assumed that members have sufficient shear and bond capacity to satisfy flexural failure. Shear capacities are checked under the developed demands later to verify this assumption.

Analysis of the frames for initial design purposes is performed by SAP2000 (CSI 2018). The moment-curvature diagram of each section was obtained and utilized along with

other essential diagrams such as the interaction diagram for each member. Base shear, story drifts, pushover curve, hysteretic curve of each element are some of the parameters monitored. The rotation of beam springs was followed to avoid exceedance of the regulation required values.

The parameters needed for earthquake design purpose following the TSC (2018) were obtained from Earthquake Hazard Map (https://www.afad.gov.tr). All the selected ground motion are far field motions. Near-fault effects are not considered of this study.

CHAPTER 2

NUMERICAL STUDY

2.1 Objective and Scope

The study planned to investigate the effect of varying column-beam strength ratio on the failure mechanism of RC moment frames. Numerical simulations are selected as the main tool to this purpose. Considering the nonlinear domain of the analysis, proper numerical models and analysis platform should be selected. OpenSees (McKenna et al., 2010) software is used for this purpose. The elected analysis platform and the simulation models are discussed in this chapter.

2.2 Open System for Earthquake Engineering Simulation (OpenSees)

OpenSees software is an open-source and object-oriented framework to simulate earthquake responses for both structural and geotechnical systems. Pacific Earthquake Engineering Research Center has supported the maintenance and improvement of OpenSees. A text file needed to be created by the user to perform the analysis. System not only permit the users to perform analysis with the provided materials and elements library but also permit the creation of new ones. Software has official webpages supported by the University of California, Berkeley for both Tcl and Python languages. The website (https://opensees.berkeley.edu) provide access to source code and the executable files. Also, information and guidance about how to write the commands and input files are available. There exists a rich collection of information in the internet from different resources as well (OpenSees Community).

OpenSees is a modular software which permits users to customize computation, simulation, visualization and data repositories. For this research, Python (https://www.python.org) programming language version was used to perform the linear and nonlinear analysis. OpenSees framework methodology is based on object-oriented and FEM (Finite Element Method). Figure 4 shows the flowchart for the FEM's framework.

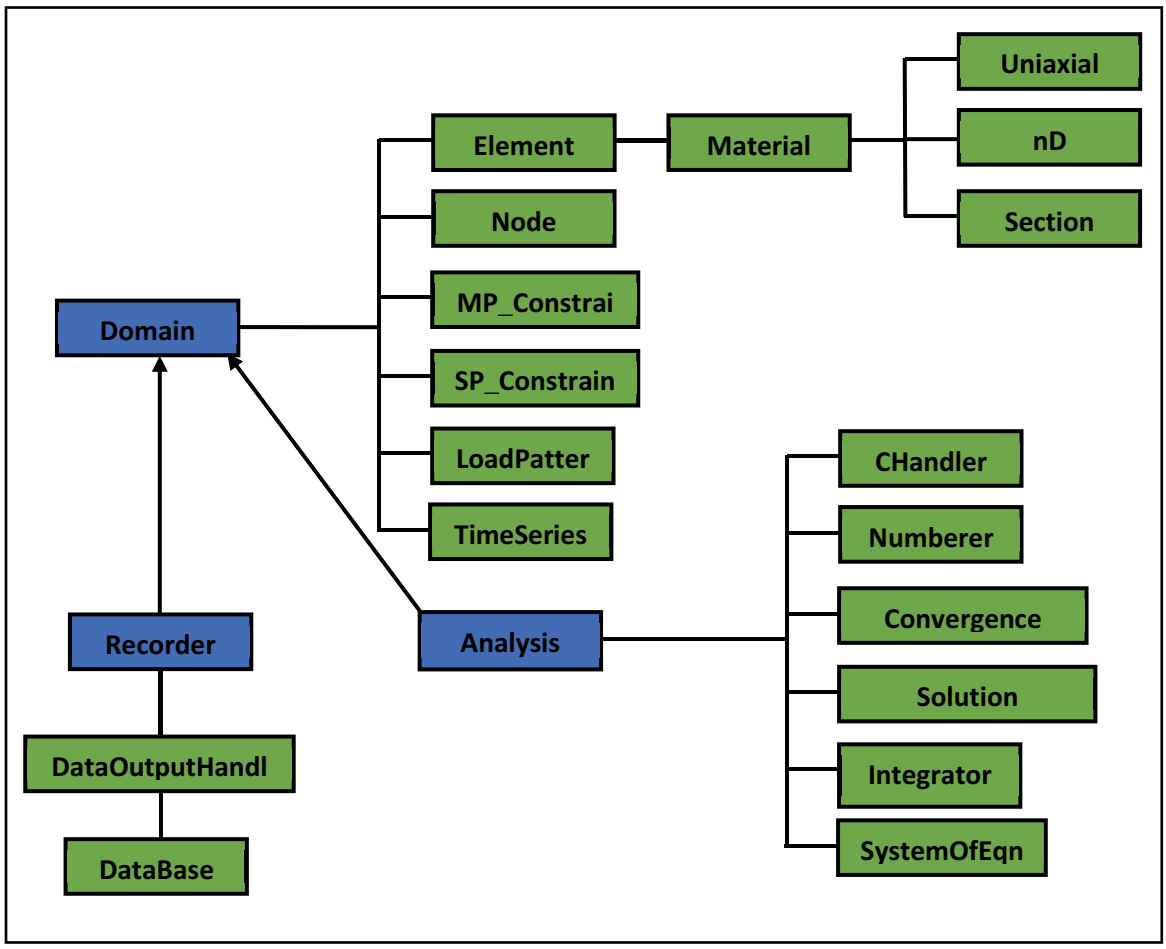

Figure 4. The package of OpenSees for finite element method

A study (McKenna et al. 2010) about the OpenSees classes shows that there are generally three types of classes to perform the nonlinear analysis of models:

1) Model Builder Classes
2) Domain Classes
3) Analysis Classes
4) Recorder

2.2.1 Model Builder

OpenSees is a strong and powerful tool for nonlinear structural assessments with its rich materials, elements, and analysis library. Due to its open-access, adaptable source code its library is keep growing with new addition. The accessibility of the source code make it a useful education tool based on the command-driven scripting language. The

architecture of the OpenSees permits the usage of all the commands as functions of each other.

OpenSees analysis needs the construction of appropriate objects and their addition to the domain. It starts with defining the number of dimensions and degrees of freedom. Nodes, elements, section properties, loads, and other objects should be defined later. The list of the most used commands available for OpenSees to perform the linear and nonlinear analysis is provided below:

- Node: Assigns coordinates to the node object
- Mass: Sets mass at node
- equalDOF: Generate a multi-point restriction between nodes.
- uniaxialMaterial: Sets material (Uniaxial Stress-Strain Relationship) to model
- Patch: Generates fibers for cross-sectional area
- Layer: Creates fibers along a line
- geomTransf: Assigns coordinate-transformation objects
- Section: Constructs a section Force-Deformation object
- Element: Assigns an element and adds to the domain
- BeamIntegration: Sets integration point to an element
- Recorder: Uses to record data
- LoadPattern: Generates loads to model
- TimeSeries: Constructs TimeSeries object for the applied load
- System: Uses to solve the equations in the analysis
- Numberer: Creates relation on how the DOF is numbered
- Constraints: Constructs Constraints handler
- Integrator: Sets integrator to determine the meaning of terms in the system
- Algorithm: Determines the sequence of steps for solving the system
- Analysis: Defines the type of analysis in the system
- Wipe: Uses to clear all constructed objected
- Test: Creates convergence test object to the system
- Analyze: Performs the analysis
- Plot: Uses to plot the diagrams and figures

- Rayleigh: Assigning damping factor to system

2.2.2 Domain Class

Classes are necessary to store the results. Domain class plays the role of a container object for the analysis. It also provides access to objects such as Node, Element, and others that were defined by the ModelBuilder object. Domain objects are shown in Figure 4.

2.2.3 Analysis Class

Generally, analysis class moves the model from a one-time step to another time step by the aggregation of component objects. The type of analysis and its implementation is conducted by component objects. Analysis objects are shown in Figure 4.

2.2.4 Recorder

A recorder object is used to save an output file of results after analysis. It could record selected information about nodes, elements, and some other objects' responses. Generally, the recorder is to be assigned before analysis commands. The recorder object flowchart is provided in Figure 4. The connectivity of the classes is presented in Figure 5.

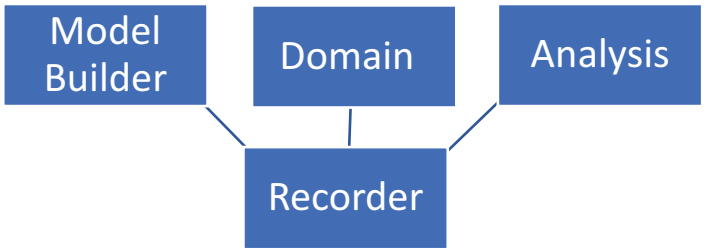

Figure 5. OpenSees classes' classification

It is necessary to select one of the optional programming languages to prepare the input file of the OpenSees. As it was mentioned before, in this study python programming language is selected. Considering that python itself is not a user-friendly software environment, an integrated development environment (IDE) is preferred to carry out OpenSees operations. PyCharm platform is chosen for this purpose. The essential Phyton libraries that are used in the analysis are as follows:

- OpenSeesPy: It is an OpenSees software interpreter.
- NumPy: It is the most widely used library for scientific calculation.
- Pandas: It is mostly used in the data science field.
- Matplotlib: It is used for dimensional plotting of numerical operations.
- SymPy: It is applied for symbolic mathematic functions.
- Scipy: Generally used for data computation and analysis.

2.3 The Selected Deterioration Model in OpenSees

A successful nonlinear time-history analysis of RC structures needs an efficient and adaptable hysteretic models. The implemented hysteretic model controls the strength, ductility, and energy dissipation of the structure. The strength deterioration of material during cyclic loading could also be implemented. Different hysteretic models are available in OpenSees, such as Takeda's model (Takeda et al., 1970), Pincheira's model (Pincheira et al., 1999), the Bouc-Wen model (Bouc and Wen, 1976) and Ibarra-Medina-Krawinkler Deterioration Model (Lignos, 2005). Ibarra-Medina-Krawinkler model is represented in Figure 6.

In this study, nonlinearity of members are modeled to be at the ends. In order to consider the effects of the variable axial loads on the moments, columns are defined have fiber discretized sections at their ends. Beams are modeled with concentrated nonlinearity with rotational springs at their ends. Rest of the both elements are accepted to be linear with a predefined effective stiffness. Backbone of the beam rotational springs (or plastic hinges) has been shown in Figure 7. It is capable of developing different strength levels in positive and negative directions. Cyclic deterioration for both positive and negative parameters, post-capping, and strain-softening could be assigned.

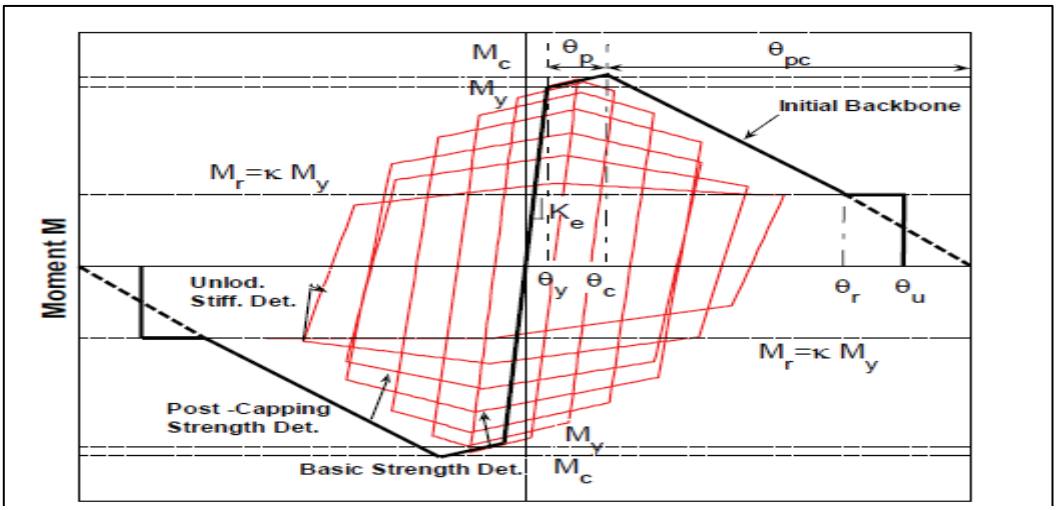

Figure 6. Modified Ibarra-Medina-Krawinkler Deterioration model with bilinear hysteretic response

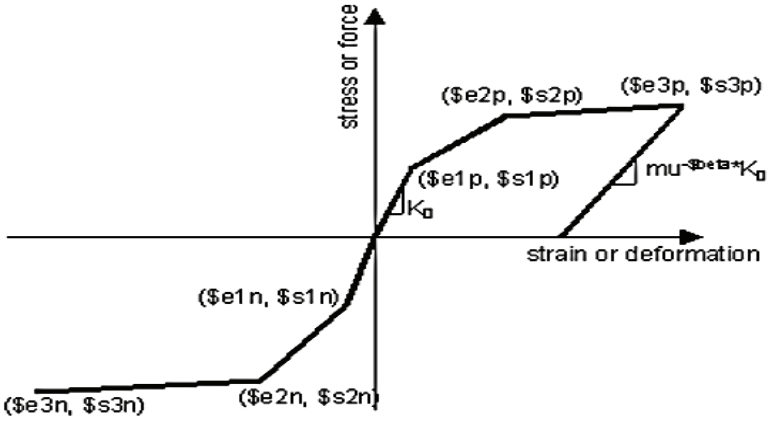

Figure 7. Hysteretic material behavior and parameters (Source: Mazzoni et al., 2006)

CHAPTER 3

NONLINEAR ANALYSIS OF REINFORCED CONCRETE MEMBERS

A general introduction about the nonlinear analysis of reinforced concrete frames will be presented. Modeling approaches such as fiber-type models and concentrated hinge models are discussed. Material presented in this chapter will provide the general framework of the procedure used to develop the analysis model for the presented study.

Seismic design philosophy is based on designing a system to develop flexure mechanism to match the demanded displacements. Since other types of mechanisms such as shear, bond failure and axial failure do not possess the required deformation capacities, system is designed to have sufficient capacities of the unwanted failure modes to enforce the flexural failure. This approach is called capacity design. Hence, modeling the flexural response properly has paramount importance in modelling the seismic response. The presentation below is developed about modelling flexural response in the nonlinear range. Currently, there are two main approaches at element and structural level. These are concentrated and distributed nonlinearity. Discussion will start with the fiber discretization of cross sections which could be utilized for concentrated and distributed nonlinearity at element level. Later concentrated hinges at the end of the members will be discussed. The properties, needed information and implementation by the Turkish Seismic Code 2018 (TSC,2018) will follow. Chapter will be finalized with the discussion of possible nonlinear analysis types for seismic design purposes.

3.1 Fiber Section Discretization

Moment curvature relation at a RC section could be calculated through slicing the section into grid (fiber model) and keeping track of the material response at each grid centroid. Both concrete and steel could be treated in a similar fashion. Assumptions of the flexural theory holds. Such an approach ensures that section could be defined from constitutive material properties. Providing the material properties and the geometry is sufficient to obtain the moment curvature relations. Another strength of the procedure is the its ability to model effect of varying axial load on the response. Hence, it could be specifically useful for members with varying axial loads such as columns under seismic excitation. It

is necessary to obtain the curvature distribution along the member to obtain the deflected shape. Members with fiber discretization could be formed either defining fiber sections on each end or defining a certain number sections along the length of the member in addition to its ends. The first approach considers a concentrated nonlinearity in the ends and the second attempted to define a distributed nonlinearity along the member.

3.2 Concentrated Nonlinearity

If it is expected to have the nonlinearity to take place at the member end zones only and the distribution of the curvature along the member could be estimated, it is possible to model a flexural member with concentrated nonlinearity at the ends. Fiber section are assigned at each end of an element to obtain the curvature at these locations. Rest of the member is accepted to stay elastic with a lowered effective stiffness. Using the curvature value obtained and an assumed length which the calculated curvature is extended (so called plastic hinge length), rotation value is obtained. Figure 8 shows the configuration of the fiber hinge model with the inelastic part at the end of the elements. The possible and idealized curvature distributions along the member are presented in Figure 9.

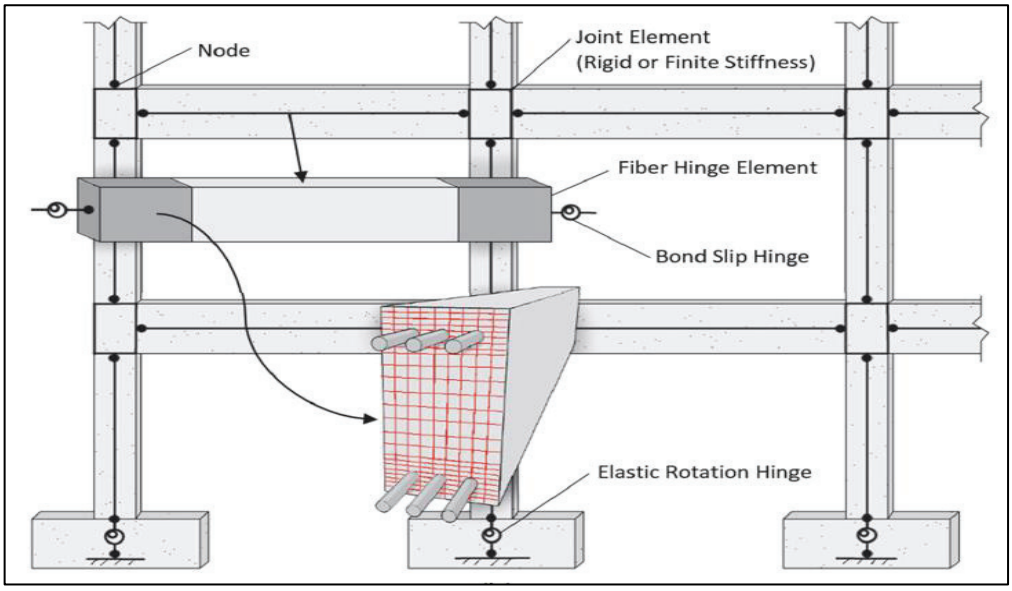

Figure 8. Overview of Concentrated Inelasticity of Fiber Elements (Source: Guidelines for Nonlinear Structural Analysis for Design buildings, NIST, 2017)

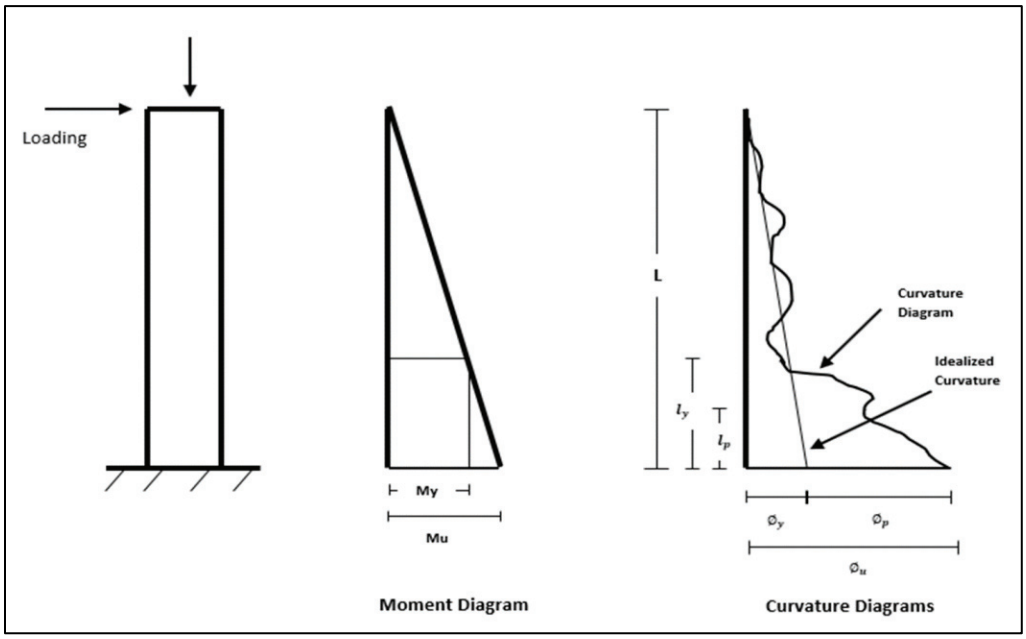

Figure 9. Schematic distribution of curvature along the member

3.3 Distributed Nonlinearity

If it is intended to define the curvature distribution along the member through calculation, it is necessary to define additional fiber sections along the length of the member. Defining such calculation points along the length provides opportunity to interpolate the curvature between these points. Simulations ranging from 3 to 7 sections are available in the literature. Figure 10 demonstrates the possible location of the fiber sections along the member.

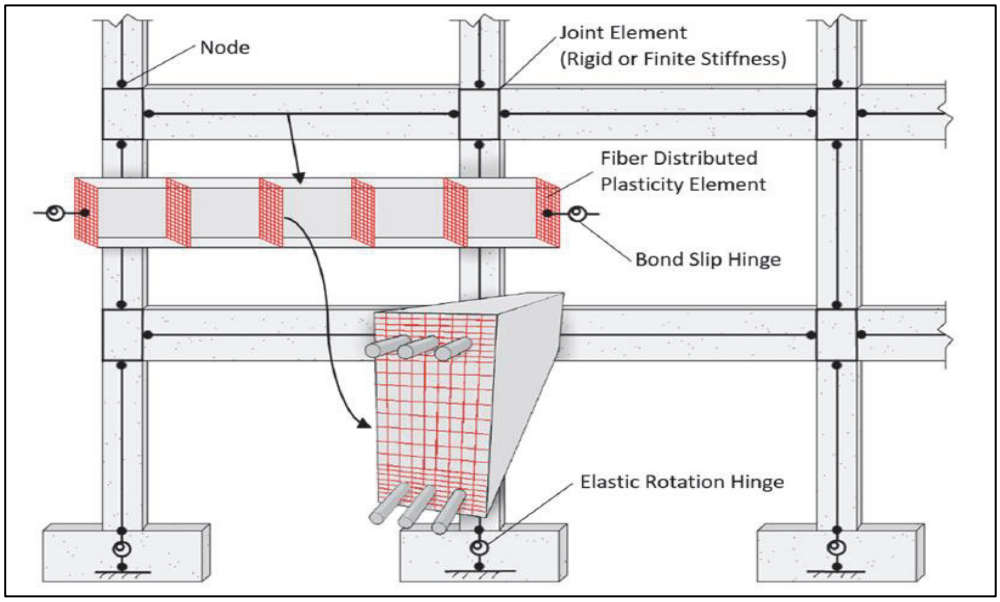

Figure 10. Overview of Distributed Inelasticity of Fiber Elements (Source: Guidelines for Nonlinear Structural Analysis for Design buildings, NIST, 2017)

Precise section properties, such as material properties and geometry, could be represented using the fiber section approach. It is possible to model any geometry of cross-section. P-M and P-M-M interaction of columns and beams and the effects on stiffness and strength could be handled with ease. The size of the stiffness matrix would stay the same which means that the DOF (degree of freedom) for each element and for overall elements are unchanged. On the other hand, the fiber-type model contains some limitations. For example, the plain section remains plain approach is assumed which misleads the analysis from true values, particularly for large strains. The typical type of fiber model do not conduct the reinforcement bond slip. It is not also able to monitor the fracture behavior and buckling of rebar. With the presence of shear-flexure interaction, it could be very

challenging to model for complicated degrading and pinching behavior. Also, it could become very costly in computing time. A comparison about concentrated and distributed fiber section plasticity could be found in Gharakhanloo (2014).

3.4 Fiber Section Modeling

For fully automated distributed plasticity models, it may not be possible obtain the needed integration weights at important locations (e.g. ends of elements). This may lead to inaccurate local curvature and deformation. A plastic hinge model could be used to overcome this limitation. The assumptions of the software's should be also taken into consideration for the location of fiber sections. For some the software, it could be possible to define the fiber section's location. For example, OpenSees (McKenna et al., 2010) permits the user to assign the exact location for the members.

If it is necessary to specify a plastic hinge length for the model, codes defined different procedures. One of the easiest ways to find the plastic hinge length, which is defined to be used by ACI318 and the TEC 2018, is to use half of the height of the section as shown below.

$$l_p=0.5h \tag{4-1}$$

h: depth of the section

Another expression also has been proposed (Berry and Eberhard, 2008) to calculate the plastic hinge length. It is based on different parameters as shown below:

$$lp= 0.05L + 0.008dbfy / \sqrt{f'c} \tag{4-2}$$

L= member length

d_b = bar diameter

f_y = steel yield strength

f'c = concrete compressive strength

Distributed plasticity can be used to predict the yielding in members when it is hard to estimate the plastic hinge such as those members with a large moment and gravity forces. Numerical localization may occur for softening components if one has used this approach

however it will work for hardening components. Then, this approach will be dependent on the number of integration points.

For cases where the plastic hinge length can be calculated, it is better to assign end elements with a known length and a small number of integration points (one or two) to have enough control for those members which shows the softening behavior. As Hachem (Hachem et al., 2003) proposed that it is more accurate to set NIP (number of integration points) in such a manner that if the plastic hinge length to member length ratio is in agreement with the integration weights of end fiber sections. To reach this approach, one needs approximately three to five NIP. In order to have better results when using displacement-based analysis, one requires to use multiple elements throughout the member if it is based on a linear-curvature assumption.

The number of fibers for each section can help to increase the accuracy of the analysis. This number will not be effective if it exceeds 5 to 10 fibers in each direction for reinforced concrete members and if it passed beyond 10 to 20 fibers, almost there will be no improvement in the behavior. However, using more fibers will also increase the computational time in most cases.

In practice, it is optimal to use smaller fibers close to the edge of sections, particularly for the reinforced concrete sections where the unconfinement exists. In addition, it will avoid convergence problems while using sensitive software. For the reinforcement generally using one fiber per rebar would be enough. Even though it is required to use rebar which is close to each other, the total area of them will be assigned as a single fiber.

3.4.1 Material For Fiber-Type Analysis

Generally, for fiber-type analysis, a uniaxial material is required to be assigned. Since a typical reinforced concrete section is made of reinforcement, confined concrete, and unconfined concrete, so three uniaxial material models are needed to represent them.

3.4.1.1 Confined Concrete – Compressive Stresses

There are different models to represent the stress-strain curve of concrete under uniaxial behavior such as Mander (Mander et al., 1988), Popovics (Popovics, 1973), and Chang and Mander (Chang and Mander, 1994). Confined concrete unlike unconfined concrete

(It will be discussed in the coming section) generally demonstrates higher strength and ductility. However, both show a hardening stress-strain behavior but are different in softening segment. A well-quality model has to contain the following properties:

- Maximum compressive strength and strain
- Maximum tensile strength and strain
- Ability to reflect the cyclic behavior for both loading and unloading
- Initial modulus changing slowly
- To show levels of confinement, having the potential of Post-Peak descending modulus

In order to define confinement for reinforced concrete sections, one needs key parameters to represent the true behavior of the section. These parameters are described as follows:

- f'_c: Concrete characteristic strength which is the strength of concrete under compression in 28 days
- f'_{cc}: Confined Concrete compressive strength
- Ɛcc: Peak confined strain
- Ɛcu: Ultimate confined strain

These parameters are depending on confinement, however, some of them can be estimated. Mander et al. (1988) and other researchers (Sattcioglu and Razvi, 1992; Ahmad and Shah, 1982; Park et al., 1982) proposed some values and formulations to estimate these parameters. For example, Ɛcc typically varies from 0.004 up to 0.01 and Ɛcu can be estimated to reach up to 0.05 or even larger for a high level of confinement, particularly for columns. Figure 11 shows the stress-strain curve in compression for both confined concrete and unconfined concrete under monotonic stress-strain (Mander et al., 1988).

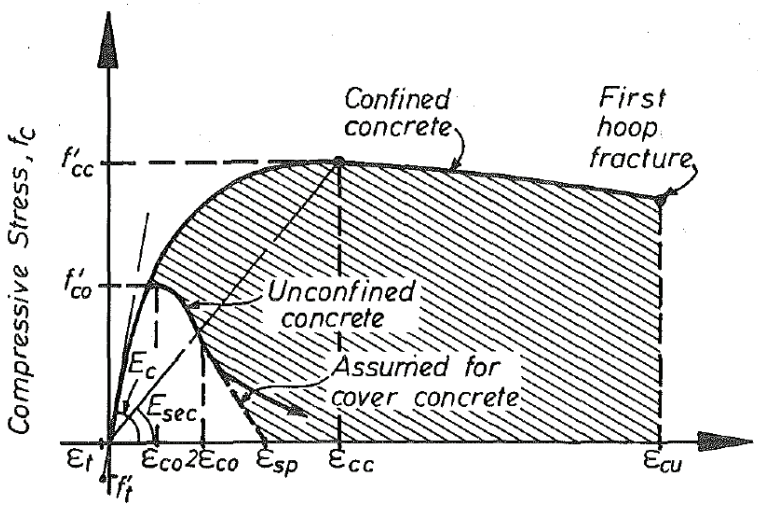

Figure 11. Confined and unconfined concrete stress-strain model (Mander et al., 1988)

$$f'c = \frac{f'_{cc}xr}{r-1+x^r} \tag{4-3}$$

$$x = \frac{\varepsilon_c}{\varepsilon_{cc}} \tag{4-4}$$

$$\varepsilon_{cc} = \varepsilon_{co}\left[1 + 5\left(\frac{f'_{cc}}{f'_{co}} - 1\right)\right] \tag{4-5}$$

$$r = \frac{E_c}{E_c - E_{sec}} \tag{4-6}$$

$$E_c = 5000\sqrt{f'_{co}}\ MPa \tag{4-7}$$

$$E_{sec} = \frac{f'_{cc}}{\varepsilon_{cc}} \tag{4-8}$$

For confined concrete, effective lateral confining pressure is defined below:

$$f'_l = f_l k_e \tag{4-9}$$

Where f_l is the transverse reinforcement lateral pressure.

$$K_e = \frac{A_e}{A_{cc}} \tag{4-10}$$

Ae = confined concrete core effective area

$$A_{cc} = Ac\ (1 - p_{cc}) \tag{4-11}$$

Where p_{cc} is the ratio of longitudinal reinforcement area to the core's area; and A_c is the area of the core of the section.

In order to calculate the effectiveness of confinement and its parameters, the following formulations have been proposed by Mander (Mander et al., 1988):

$$K_e = \frac{\left(1-\sum_{i=1}^{n}\frac{(w\prime_i)^2}{6b_c d_c}\right)\left(1-\frac{s\prime}{2b_c}\right)\left(1-\frac{s\prime}{2d_c}\right)}{1-\rho_{cc}} \tag{4-12}$$

The above equation parameters are provided in figure 12. For the circular section, the process has been described by Mander et al. (1988).

Confined concrete compressive strength (f'cc) can be computed using the equation (4-13) and using figure 13.

$$f'_{cc} = f'_{co}\left(-1.254 + 2.254\sqrt{1 + \frac{7.94\, f'_l}{f'_{co}}} - 2\frac{f'_l}{f'_{co}}\right) \tag{4-13}$$

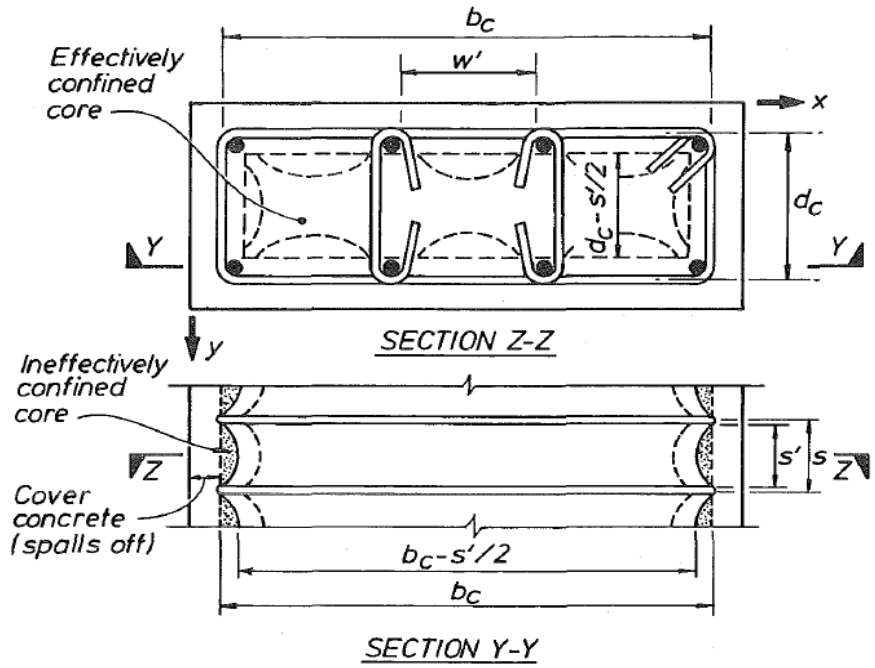

Figure 12. Parameters definition for rectangular transverse reinforcement of effectively confining core (Mander et al., 1988)

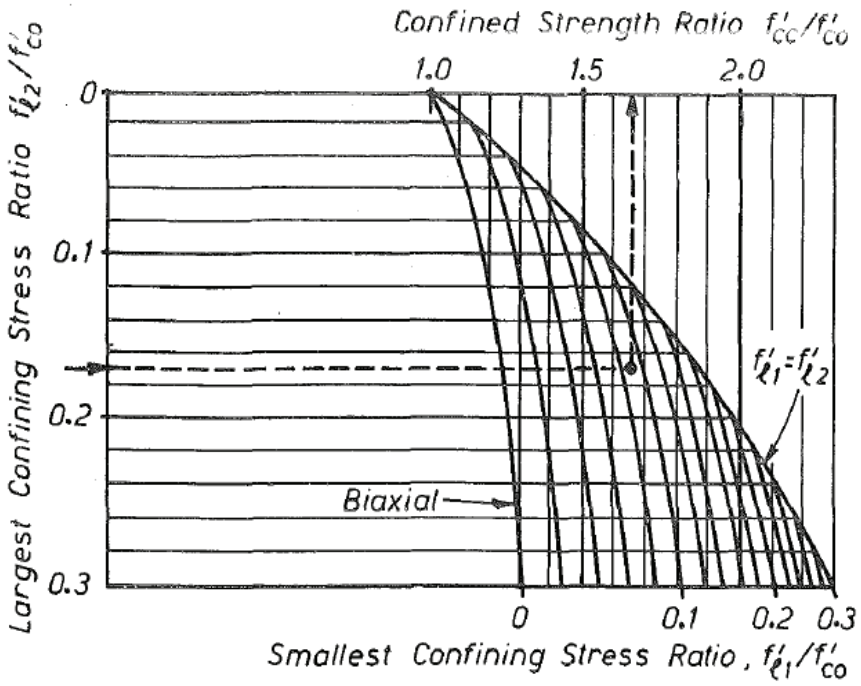

Figure 13. For rectangular sections, determination of confining from lateral confining stresses (Mander et al., 1988)

The ultimate confined concrete strain can be calculated by equation (4-14). This formulation was proposed by Pauly and Priestly (1992) to estimate it conservatively.

However, Mander also developed a method for computing ε_{cc} based on an energy balance equation.

$$\varepsilon_{cu} = 0.004 + 1.4 * \rho_s \, f_{yh} \varepsilon_{su} / f'_{cc} \quad (4\text{-}14)$$

where ε_{su} is the ultimate strain of transverse reinforcement

3.4.1.2 Unconfined Concrete – Compressive Stresses

The unconfined concrete model which represents the concrete excluding the transverse reinforcement has been developed by different researchers. There are different models for this purpose as mentioned in the previous section. These model parameters are the same as confined concrete except for strength and ductility parameters. Confined concrete is more ductile and has a higher strength capacity compared to unconfined concrete. The essential parameters for defining the unconfined concrete are listed below:

- f'c: Concrete characteristic strength which is the strength of concrete under compression in 28 days
- Ɛco: Peak unconfined strain
- Ɛsp: Spalling strain

The value of $Ɛ_{co}$ is between 0.002 to 0.003 but typically it is taken as 0.003. The spalling strain is around $2Ɛ_{co}$; however, it is not too critical to monitor the response while considering it. These values were based on studies which were conducted by researchers mentioned in the previous section. Figure 5 shows the stress-strain curve in compression for unconfined concrete together with confined concrete under monotonic stress-strain (Mander et al., 1988).

3.4.2 Concrete Material in OpenSees

There are several types of concrete materials in OpenSees software. The most common ones are listed below:

- Concrete01
- Concrete04
- Concrete06

Concrete01 is based on Kent-Scott-Park (Kent & Park, 1971) and Karsan and Jirsa (1969) concrete uniaxial material and has no tensile strength (see Figure 14 and 15). Concrete04 represents the Popovics uniaxial concrete material and Karsan and Jirsa (1969) studies and contains tensile strength. Concrete06 is a uniaxial concrete material with nonlinear tension stiffening, tensile strength, and Thorenfeldt curve.

In this study, concrete01 was used to demonstrate the concrete behavior under imposed forces. As mentioned above, this material is a uniaxial Kent-Scott-Park (1971) object containing unloading and reloading stiffness considering Karsan and Jirsa (1969) work. It has no tensile strength. The parameters for this material should be assigned as negative values in the OpenSees platform.

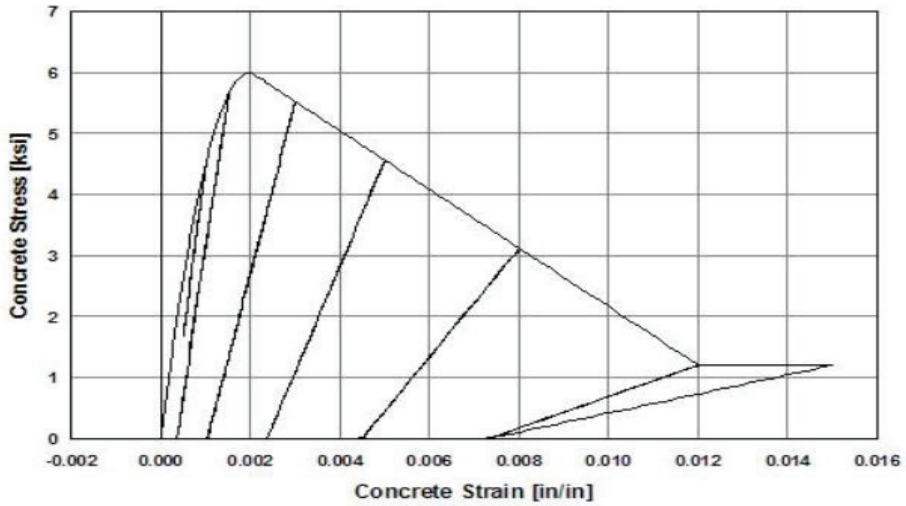

Figure 14. Stress-Strain diagram of Concrete01 (Source: Mazzoni et al., 2006)

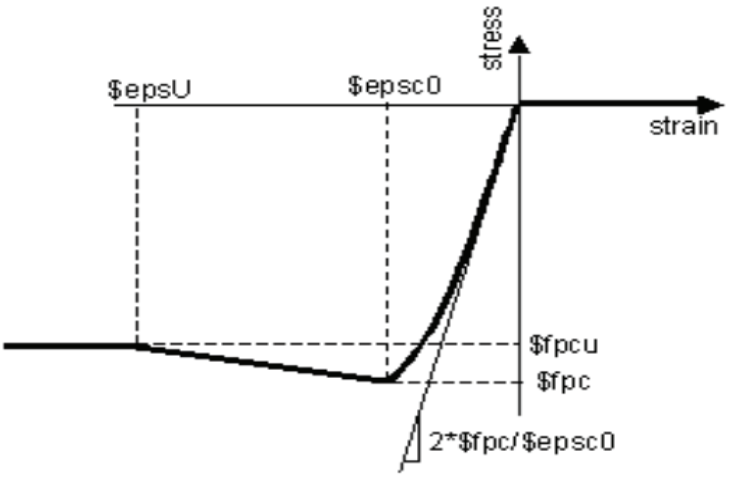

Figure 15. Concrete01 typical Hysteretic Stress-Strain Relation (Source: Mazzoni et al., 2006)

3.4.3 Steel Reinforcement in OpenSees

Generally, the steel reinforcement for the analysis should have some properties in order to match the real case. These properties depend on what type of analysis is going to be used. Some of these properties can be essential however some others might not affect the analysis. Here is the list of important properties as follows:

- The reinforcement material has to have an elastic response that can be driven from initial the modulus
- Post-yielding plateau
- Strain hardening which can be optional
- Bauschinger effect
- Cyclic isotropic hardening

There are several types of uniaxial materials (force–deformation relationship) developed for OpenSees software. The three common ones are described below:

- Steel01: It contains bilinear steel material with hardening
- Steel02: This material is based on Giuffre-Menegotto-Pinto studies
- Steel04: This material has combined isotropic and kinematic hardening

In this study, Steel02 has been used for analysis. As was already mentioned, this model indicates Giuffré-Menegotto-Pinto (Giuffrè, 1970; Menegotto & Pinto, 1973) research which accounts for the strain hardening. The ratio was taken as 1% for strain hardening in this study while other parameters were applied as software defaults. Figures 16 and 17

show the monotonic and hysteretic response of Steel02 respectively. For more information about the behavior of this material, one can visit OpenSees' official website known as "OpenSeesWiki".

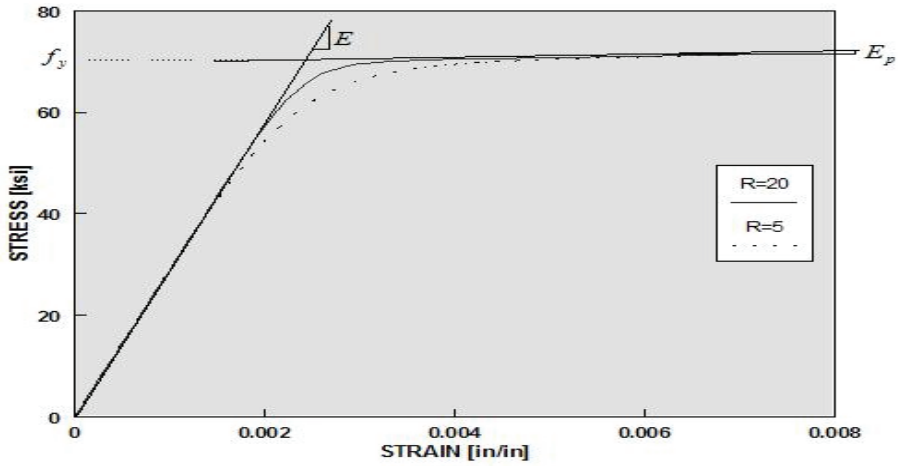

Figure 16. Steel02- Monotonic Envelope (Source: Mazzoni et al., 2006)

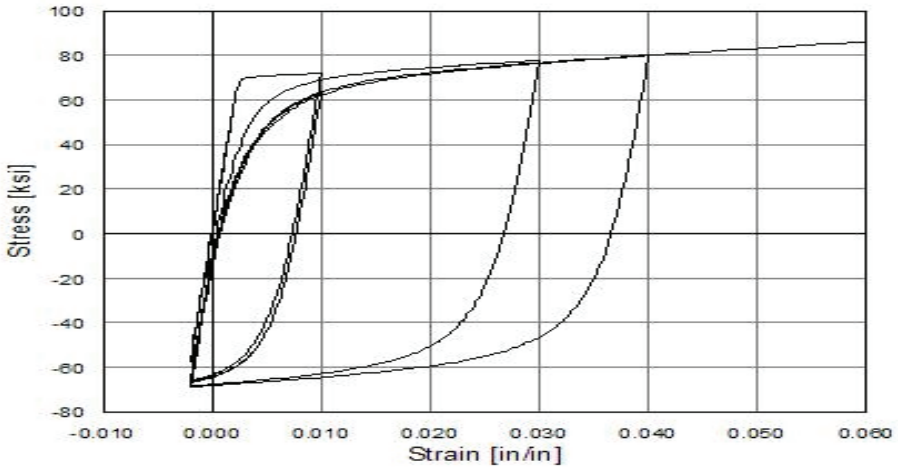

Figure 17. Steel02- Hysteretic response with Isotropic Hardening (Source: Mazzoni et al., 2006)

3.4.4 Concentrated Hinge Model

One of the simple and efficient methods to investigate the behavior of column and beam members in nonlinear analysis is to use concentrated hinge models. In this model, a zero-length member which typically is known as a rotational spring is added at the end of members to monitor the inelastic response and an elastic line element is then connected

to this spring to represent the elastic stiffness of this member. Figure 18 shows the concentrated hinge component models.

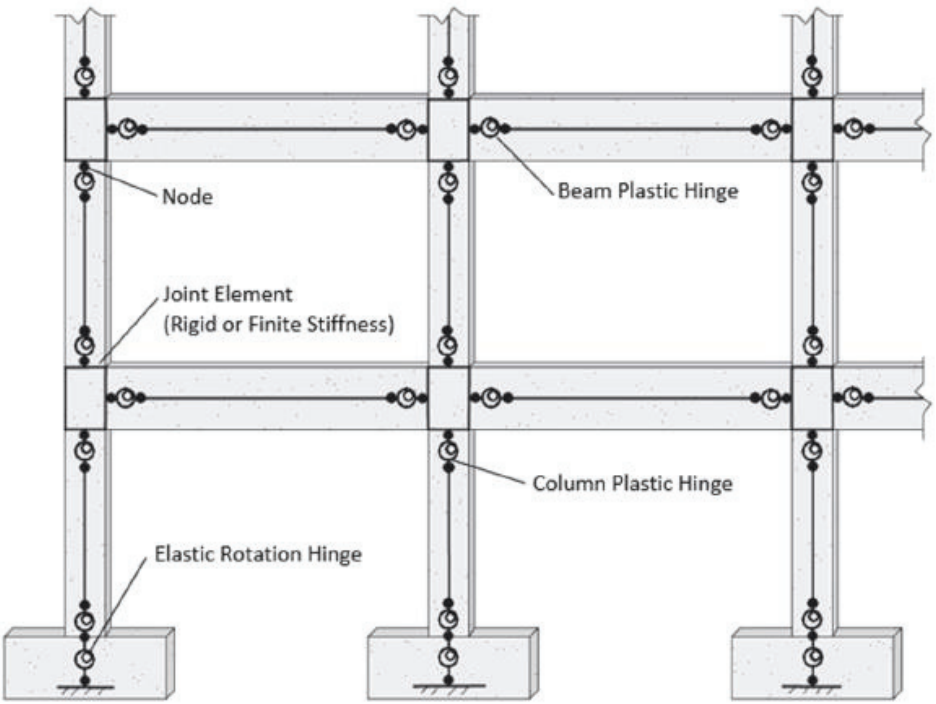

Figure 17. Concentrated hinge model in a moment-resisting frame (Source: Guidelines for Nonlinear Structural Analysis for Design buildings,NIST,2017)

This approach might be more challenging if the inelastic deformation's location is not clear. Stress-strain relations are performed considering average boundary conditions and the influence of axial load variations particularly on column stiffness and strength cannot be monitored properly during the assessment.

To simulate the response of this type of hinge, the idealization of the moment-rotation relation can be conducted as shown in figure 19. The force-deformation capacity can be then derived from this curve. This curve includes the yield moment and rotation, the maximum moment and rotation, and the post-capping rotation considering residual strength. It can be performed for both monotonic and cyclic analysis. For monotonic analysis, the response of the rotational spring will be as an envelope curve. On the other hand, for cyclic assessment, the reduction in strength and deformation capacities would happen for the inelastic range. It might even reach the first-cycle backbone for many

cycles' performance. The detail shown in figure 15 is to predict the column or beam responses in a way for every type of modeling.

Nojavan (after Nojavan et al., 2014, 2016) has conducted a test to see the similarities between the cyclic and monotonic responses of a system. It has shown in Figure 20 that both types of loading are almost alike for fewer cycles. However, for a larger number of cycles, this approach may lead to a bit of difference.

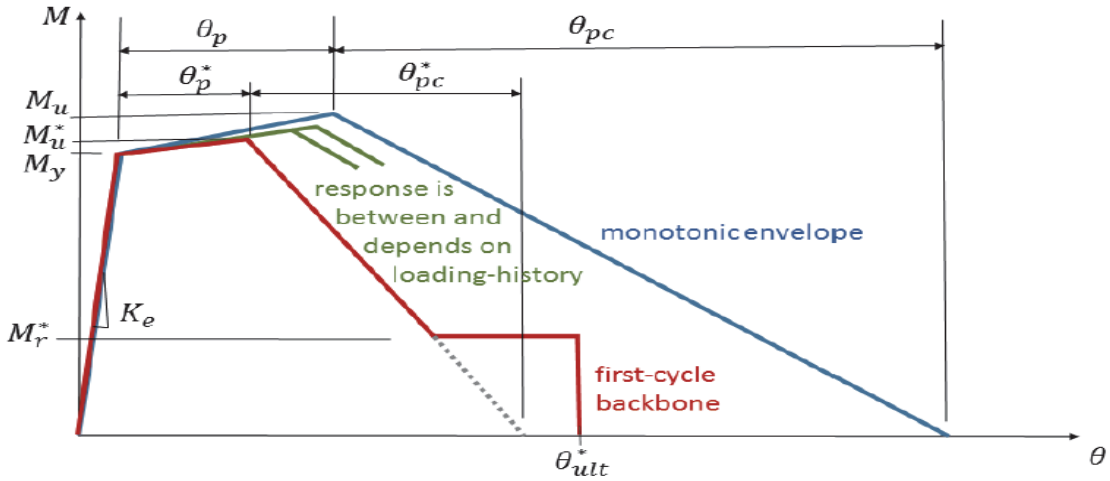

Figure 18. Idealized moment-rotation response of a column. Adapted from figure 2-5 (NIST,2017)

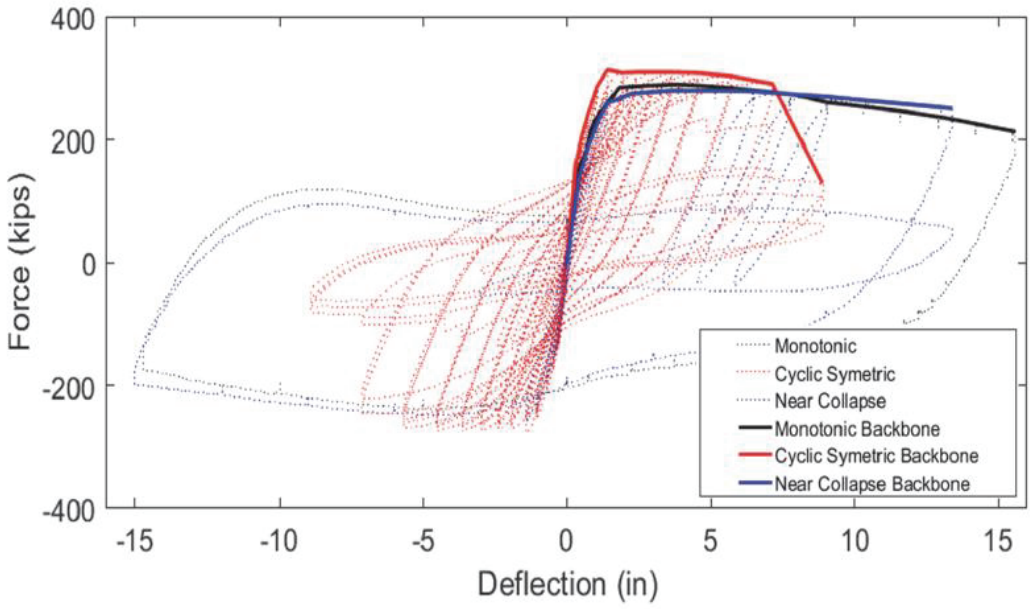

Figure 20. The monotonic, cyclic and near-collapse loading (after Nojavan et al., 2014,2016)

In this study, a rotational spring that represents the moment curvature relationship was assigned at the end of each beam's end to simulate the real behavior of the reinforced concrete section due to pushover and cyclic loading. This material is known as "Hysteretic" in OpenSees material types. Afterward, The rotational spring reactions are monitored to find the response of the beam. The essential output of this spring is moment and rotation. Figure 19 shows a typical bilinear behavior of this material.

3.4.5 Moment-Curvature Analysis

Moment curvature analysis is a method to define the maximum capacity of a structural section whose failure mode is flexural. Its diagram (Figure 21) demonstrates the ductility and the energy dissipation capacity of the section. This process uses the nonlinear material stress-strain relationship of the section to accurately determine the load-deformation response of the section. Different parameters can change the moment-curvature diagram such as material type, axial load, cross-section, confinement, and for a more accurate response, the integration point. These parameters can be applied to software to calculate the capacity of the section.

Layer-by-layer analysis of the section can also be conducted. In a rectangular section, one can divide the section into "n" number of sections as shown in figure 22. The section particularly contains two zones; confined and unconfined zones. The stress and strain of these zones are calculated and assigned to software to perform the nonlinear analysis.

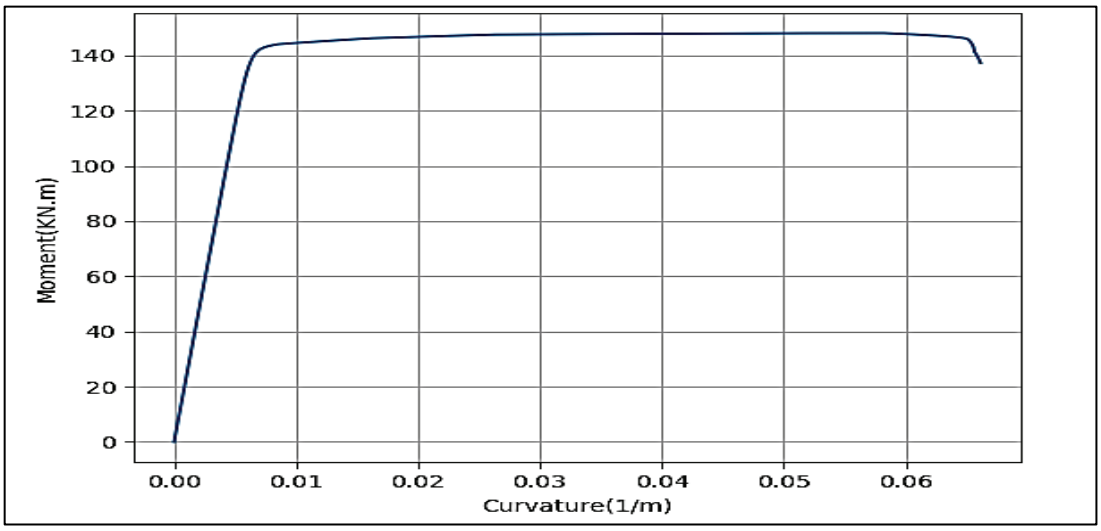

Figure 21. Moment-Curvature diagram of a typical beam section drawn by OpenSees

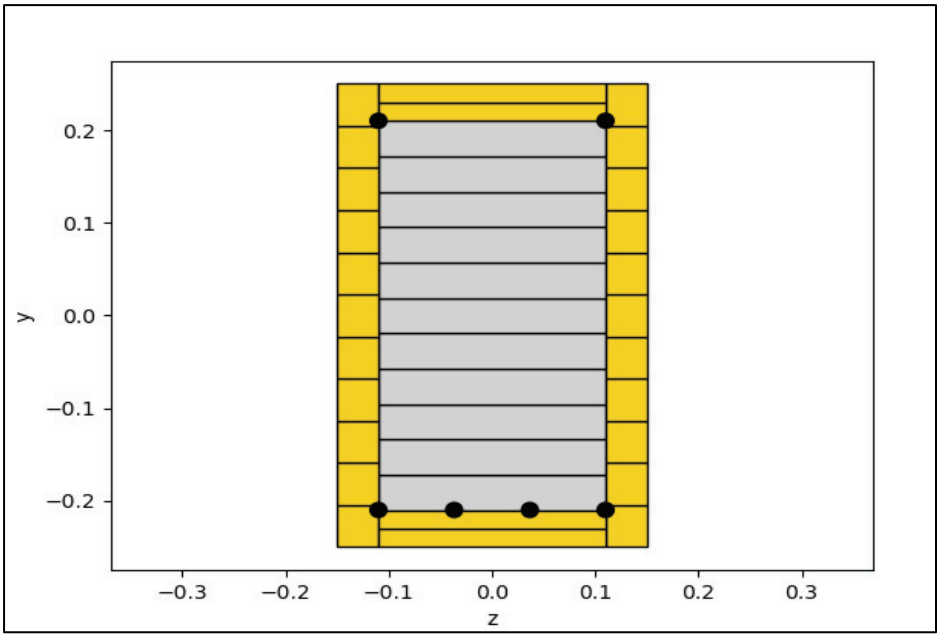

Figure 22. Layer by Layer division of a typical beam section drawn in OpenSees

Many software has the capability to perform the moment-curvature analysis. OpenSees (McKenna et al., 2010), SAP2000 , XSECTION, CONSEC, and Response2000 are generally used for this purpose. In this study, the OpenSees framework and an Excel sheet created by Ersoy et al (2000) are used to carry out the moment-curvature analysis of the sections. Fiber section is utilized for all columns in this research.

However, rotational springs are used at the end of each beam (see Figure 18), therefore the usage of moment-curvature is more crucial for these elements. The capacity of beams is calculated using moment-curvature analysis and then it is assigned to rotational springs to represent the capacity of beams. Figure 21 shows the moment-curvature diagram of a simple beam using OpenSees software.

The data from the moment-curvature diagram then can be converted to desired formats. One may need the force-deformation results, so it can be used for that purpose or if a moment-rotation diagram or data are required, it can be converted basically by multiplying the curvature by the plastic hinge length of the section. In fact, moment-curvature analysis is the inelastic response of the section considering the material's behavior. Figure 23 shows a moment-rotation diagram of a column section.

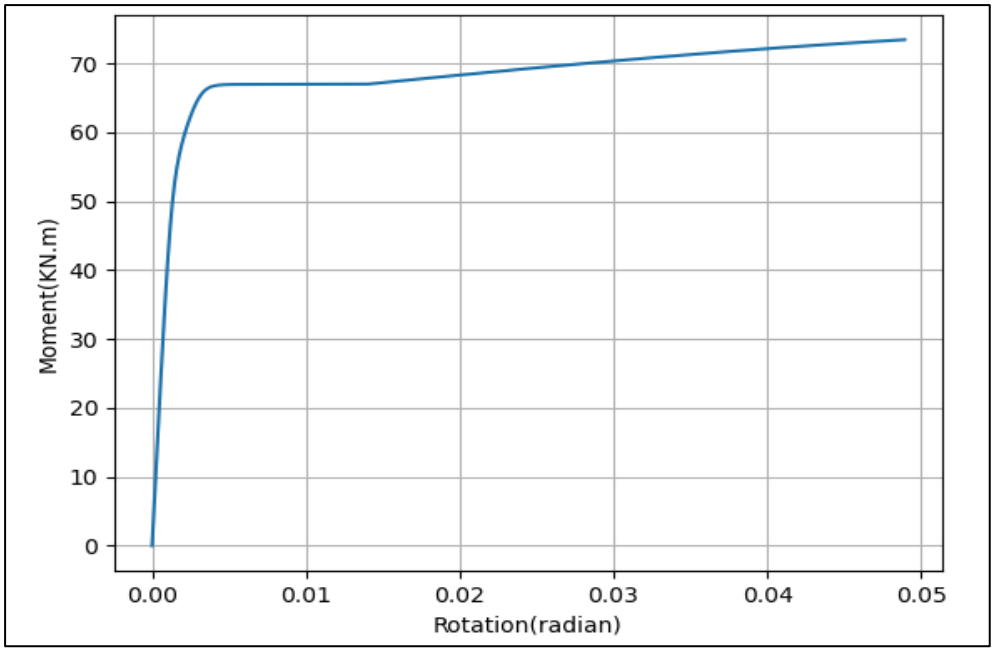

Figure 23. Moment-Rotation of a typical Column drawn by OpenSees

3.4.6 Seismic Performance Levels

In TSC 2018, there are four types of performance levels.

- Immediate Occupancy
- Life Safety
- Collapse Prevention
- Collapse

In the immediate occupancy (IO) level of performance, 10% of beams at one story may be in moderate damage and the rest in slightly damaged condition. The overall damage is light. The structure almost keeps its original stiffness and strength.

For life safety (LS) performance level, 30% of the beams are allowed to be heavily damaged and the rest should be in good condition. In addition, the columns' shear force in the heavily damaged zone should not exceed 20% of the total shear force for the story. The overall damage to this level is moderate. There will be some loss in stiffness however, the gravity- load carrying elements and some lateral strength will be functioning.

The structure will lose its significant strength and stiffness in the collapse prevention (CP) level of performance. However, columns, shear walls, and other elements which are responsible for gravity load carrying will be still operational. The overall damage is

severe. In this level except for 20% of beams that are in the collapse region, the rest may be slightly damaged or heavy. On the other hand, the shear force level should not exceed 30% for those columns that are beyond the damaged region. The collapse level of performance is when the building is not functioning.

3.4.6.1 Failure Limits in TSC 2018

In TSC 2018, for rectangular sections in the failure prevention level, the following strain limitation is given for the concrete:

$$\varepsilon c^{GÖ} = 0.0035 + 0.04\sqrt{\omega_{we}} \leq 0.018 \quad (4.1)$$

Where ω_{we} mechanical reinforcement ratio of effective winding reinforcement and can be found using the below formula:

$$\omega_{we} = \alpha_{se}\,\rho_{sh,min}\,\frac{f_{ywe}}{f_{ce}} \quad (4.2)$$

αse: Winding reinforcement efficiency coefficient

ρsh, min: The smaller of the volumetric transverse reinforcement ratio in the two horizontal

directions in the rectangular section

*f*ywe: The expected transverse reinforcement yield strength

fce: The expected concrete yield strength

α se can be calculated using equation 4.3:

$$\alpha_{se} = \left(1-\frac{\sum a_i^2}{6b_o h_o}\right)\left(1-\frac{s}{2b_o}\right)\left(1-\frac{s}{2h_o}\right) \quad ; \quad \rho_{sh} = \frac{A_{sh}}{b_k s} \quad (4.3)$$

A_{sh}: The area of transverse reinforcement

b_k: core length in the vertical direction (between the outermost transverse

reinforcement)

s: Spacing between transverse reinforcement

b_o and h_o: The wrapped concrete dimensions measured from the wrap reinforcement

axes

a_i: Indicates the distance between the axes of longitudinal rebar supported by a stirrup or cross tie

For steel reinforcement (S420) the following equation can be utilized:

$$\varepsilon_s^{(GÖ)} = 0.4\varepsilon_{su} \tag{4.4}$$

ε_{su}: Elongation per unit corresponding to the tensile strength

The plastic rotation limit for failure prevention according to TSC 2018 is given below:

$$\theta_p^{(GÖ)} = \frac{2}{3}\left[(\phi_u - \phi_y) L_p \left(1 - 0.5\,\frac{L_p}{L_s}\right) + 4.5\,\phi_u\, d_b\right] \tag{4.5}$$

ϕ_u : Ultimate curvature

ϕ_y : Yield curvature

L_P: Plastic hinge length (In TSC 2018, Lp = 0.5h)

L_s: Shear span

In the Turkish seismic code (TSC 2018), there are other important limits known as "Damage Control Limits". Equations (4.6), (4.7), and (4.8) are utilized to find concrete, steel, and plastic rotation limits respectively.

$$\varepsilon_c^{(KH)} = 0.75\,\varepsilon_c^{(GÖ)} \tag{4.6}$$

$$\varepsilon_s^{(KH)} = 0.75\,\varepsilon_s^{(GÖ)} \tag{4.7}$$

$$\theta_p^{(KH)} = 0.75\,\theta_p^{(GÖ)} \tag{4.8}$$

The control point for Limited Damage is also provided below according to TSC 2018. These equations are used to calculate the damage limits for concrete, steel, and plastic rotation respectively.

$$\varepsilon_c^{(SH)} = 0.0025 \tag{4.9}$$

$$\varepsilon_s^{(SH)} = 0.0075 \tag{4.10}$$

$$\theta_p^{(SH)} = 0 \tag{4.11}$$

3.4.6.2 Turkish Earthquake Code Material Limit

Turkish Earthquake Regulation (TER, 2018) provides limitation for the material. With the aid of this limitation, one can find the performance level of the structure after seismic assessment. Figure 24 shows the damage zone according to TER (2018).

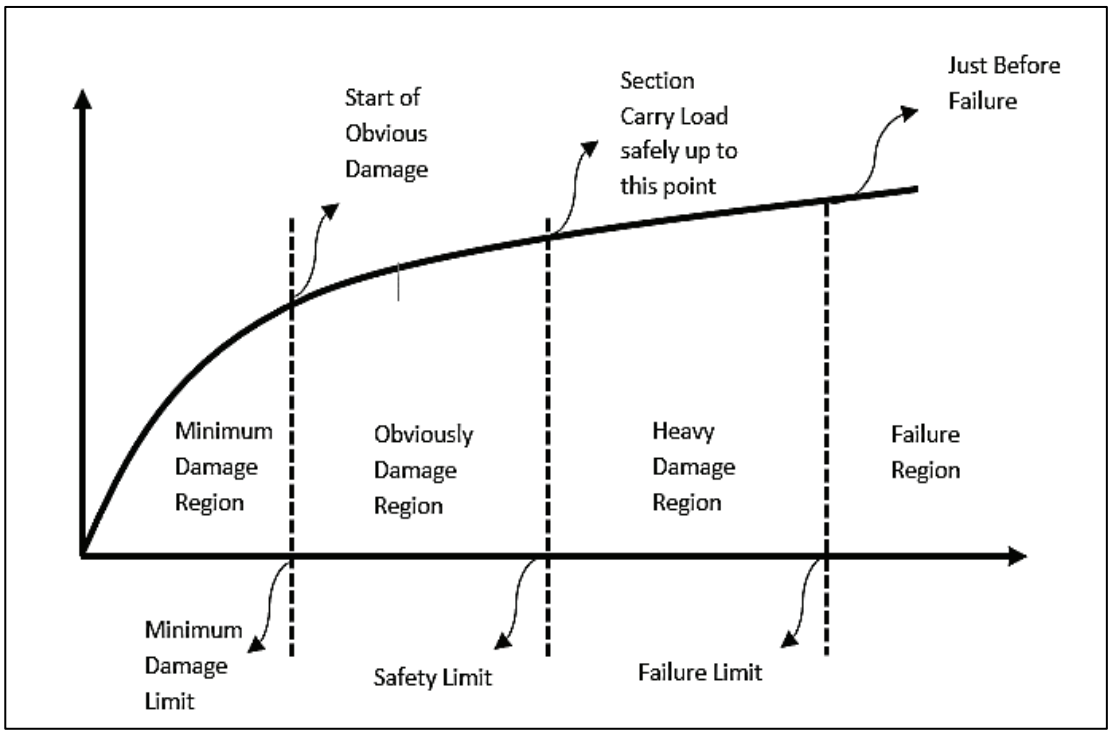

Figure 19. Material Limit according to TSC 2018

3.4.7 Pushover Analysis

During the past twenty years, pushover analysis has evolved into the preferred method for the evaluation and design of seismic systems and buildings in response to earthquakes, since it is relatively simple and incorporates post-elastic response. The reliability of this type of analysis for all structures has been a topic of discussion and improved pushover procedures have been proposed to overcome some of the restrictions considering new methods.

Pushover analysis is a static approximate method that utilizes nonlinear techniques to estimate and monitor the behavior of structure imposed to increasing lateral force with a particular distribution in height up to reaching a target displacement. To approximate a force-displacement curve of the overall structure, pushover analysis contains a series of sequential elastic analyses. Initially, a two or three-dimensional model is created and then the gravity load is applied. The lateral loads are then distributed along the building height in accordance with a predefined pattern. Increasing lateral forces cause some members to yield. As a result of the reduced stiffness of yielded members in the structural model, the lateral forces are re-increasing until additional members yield as well. Generally, the roof displacement together with base shear is plotted to get the capacity curve (Figure 25).

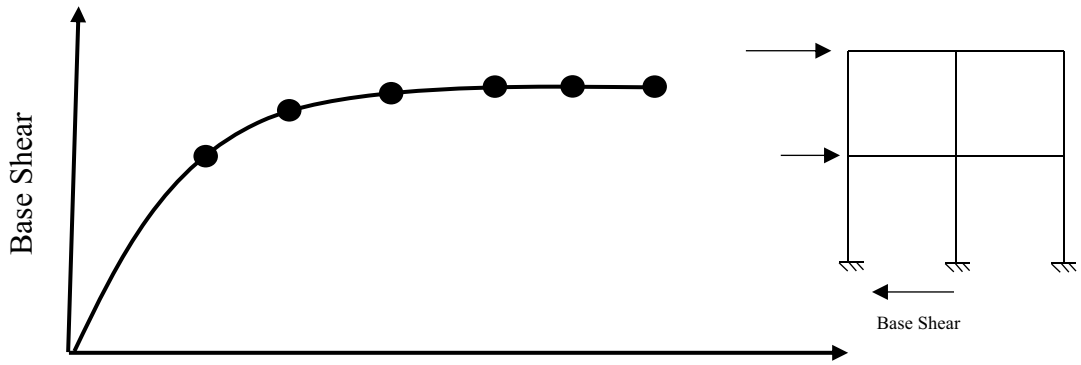

Figure 20. Capacity curve of a structure

There are two types of ways to perform the pushover analysis:

- Force-Controlled
- Displacement-Controlled

For the force-controlled procedure, the load should be known. The specified load combination will be applied to the model. In this method, some numerical problems may

impact the results due to small negative or positive lateral stiffness caused by P-Delta effects and developed mechanisms.

Displacement-controlled which was proposed by Allahabadi (Allahabadi R., 1987) is the general procedure to implement the pushover analysis and get rid of the above problems. In this method, a displacement is specified and the load magnitude is not known. The applied load to the model is increased until reaching the targeted displacement. Roof displacement at the top node or at the center of mass is picked out to perform the nonlinear analysis. Considering the roof displacement and base shear model, one can plot the capacity curve of the model.

The performance check of the system can be conducted after the estimation of inelastic deformation and strength of the model using the calculated internal forces and deformations. Pushover analysis makes it possible to trace and monitor the sequence of yielding and failure for each structure's element until performing the complete capacity curve (Figure 25). This method provides information about the behavior of the whole structure and individual elements which cannot be grasped using elastic analysis.

The following information can be achieved using pushover analysis:

- Deformation demand for ductility
- Estimation of inter-story drifts' distribution
- Strength deterioration of members
- Estimation of inter-story drift
- Determining the failure mechanism of the structure
- Exposes the design weakness

The accuracy of pushover depends on many parameters such as:

- Selection of load pattern
- Failure mechanism
- Target displacement

The selected load pattern should represent the inertial forces imposed on the structure during the seismic performance. Typically, an invariant lateral load pattern is used in the analysis where the distribution of inertia forces is assumed to be constant during the earthquake and the deformed shape of the model under the action of these loads is

expected to be similar to a real earthquake. Lateral load pattern preference is more crucial compared with target displacement estimation.

Turkish seismic code (TSC 2018) provides an equation to find the applied load to the model. This load is generally in triangular shape. Equation 4.12 is used to find the forces at story levels:

$$F_i = (V_t - \Delta F) * \frac{m_i * H_i}{\sum_{j=1}^{N} m_j * H_j} \quad (4.12)$$

V_t: total equivalent earthquake load

ΔF: parameter for considering the effect of higher mode

mi: i^{th} floor mass

Hi: i^{th} floor height

ΔF can be calculated using the following equation:

$$\Delta F = 0.0075 * N * Vt \quad (4.13)$$

N: Number of stories

ΔF will be applied at the top floor level as shown in Figure 26.

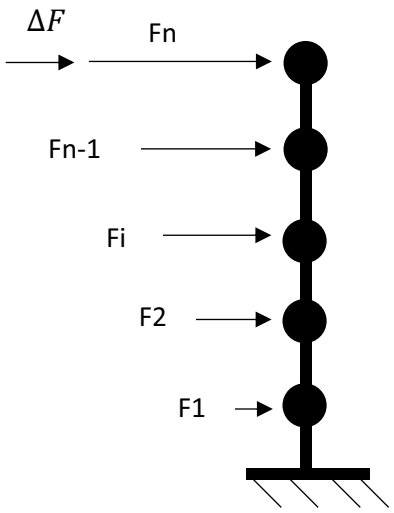

Figure 21. Forces at different story levels

3.4.8 Time History Analysis

Nonlinear dynamic analysis or time history analysis is a step-by-step assessment of the dynamic behavior of a structure subjected to time-varying load. This is the most accurate and realistic way available for representing seismic analysis of a structure under dynamic loading. It is also known as “nonlinear response history analysis” or “nonlinear dynamic procedure” according to ASCE 41-13 (2013). In order to conduct such an assessment, a representative earthquake time history data is needed.

Seismic loading is represented by application of ground motion acceleration time history (see Figure 27 for an example of ground motion record) on a model that is capable of simulating the inelastic behavior of structural elements and geometric nonlinearity (P-Delta effects). Response histories for any required parameter (e.g., displacement or stresses) could be obtained throughout the structure. Since the selected ground motion records may produce demands that change considerably, typically a set of ground motion records that is accepted to represent the envelope design spectra is selected. Furthermore, to figure out different regimes of structural response or failure, one can utilize more than one level of seismic intensity.

Ground motion records can be expressed in the form of following parameters at a site:

- Displacement
- Velocity
- Acceleration

In general, in a strong ground motion, accelerations are recorded and then the velocity and displacement are calculated.

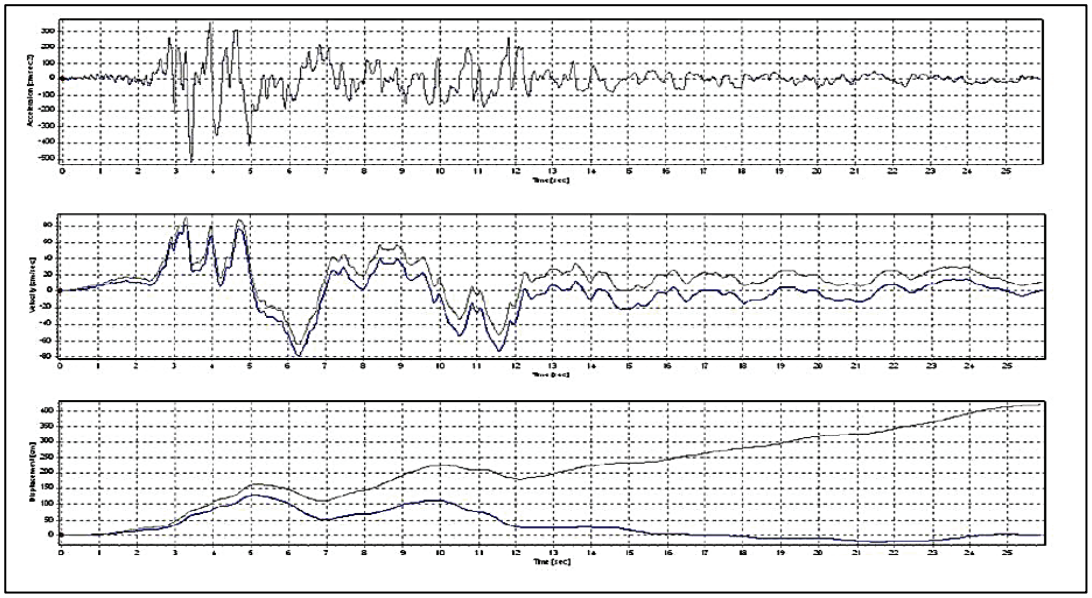

Figure 22. Ground motions recorded during earthquake in Düzce on 12 November 1999, (source: Peer Website)

CHAPTER 4

DESIGN OF THE SIMULATED FRAMES

4.1 Introduction

The design decisions and the process of the 2D frames that are used in this study is presented in this chapter. This study examines three-bay two-story, five-story, and eight-story planar frames. Each frame consists of a frame analyzed and designed using conventional seismic method. Turkish Earthquake Regulation (TER 2018) and the Turkish Reinforced Concrete Standard (TS 500, 2003) are used in the design. A pushover and time-history analysis were performed to monitor the behavior of each frame considering the plastic hinge occurrences in both beams and columns. Different strong-column weak-beam design ratios were selected ranging from 1.2 up to 4.0. The results of each frame's behavior are also presented in this chapter.

The selected frames for all case studies have different heights but similar plans. Frames are considered to be part of buildings with typical spans as shown in Figure 28. The 2D frames used in simulations are typical internal frames of these prototype structures. Such a plan and the selected 2D frame are shown in Figure 28.

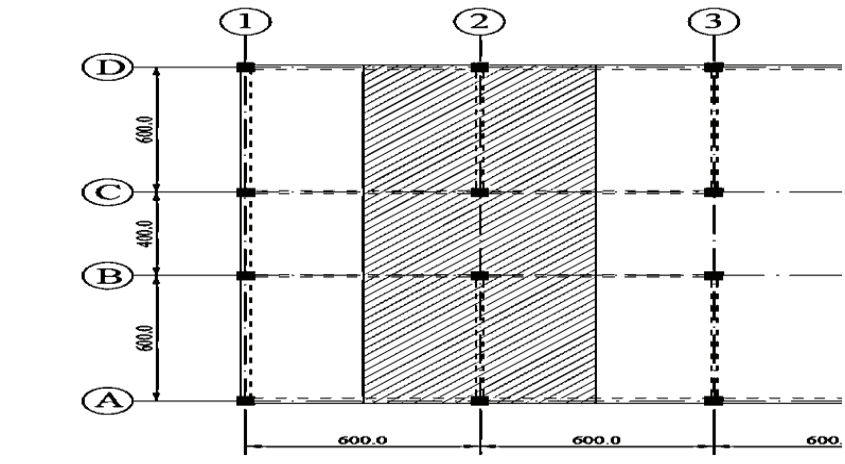

Figure 23. Typical plane for the case studies, dimensions are in cm.

The beams are designed as doubly reinforced concrete beams for flexural purposes. The section analyzer used for this purpose was an spreadsheet and the corresponding moment

curvature was created using the spreadsheet coded by Ersoy et al. in 2000 and OpenSees (McKenna et al., 2010). Information about the spreadsheet is available in Ersoy et al. (2013). The design moments that were used in this program are the moments at the column faces., the restrictions for reinforcement ratios, as recommended in TS500 and Turkish Seismic Code (2018), are taken into account in this program.

The purpose of shear design for structural members in seismic regions is to prevent failures due to shear, and ensure failures in flexure (i.e. if failures occur, they should be due to flexure failure, not shear failure). For this purpose, one should follow all the requirements in the Turkish Seismic Code (2018). An spreadsheet was created to check all these recommendations and requirements.

There could be several load types acting on the structure at the same time, hence load combination should be considered. These loads can be dead, live, seismic, wind, or snow loads in most cases. As a result of a variety of load combinations and load factors specified by building codes and regulations, the structure should be safe under a variety of maximum expected loads. In this study, three types of load combinations have been used. These loads contain seismic, dead and live effects that are applied to the model as shown below with their corresponding factors.

$$F_d = 1.4G + 1.6Q$$
$$F_d = 1.0G + 1.0Q + 1.0E \qquad 5.1$$
$$F_d = 0.9G + 1.0E$$

Where:

G is the dead load

Q is the live load

E is the earthquake load

In accordance with TER (2018), the primary design of frames was conducted using equivalent lateral load method along with capacity design principles. It is assumed that the frames are located in a high-seismicity area that contains ZD soil type (Figure 29). Using the Turkish Earthquake Risk Map (AFAD), the linear elastic acceleration design

spectrum was attained that the probability of exceeding is 10% in 50 years. Figure 30 demonstrates the linear elastic design spectrum of the chosen site.

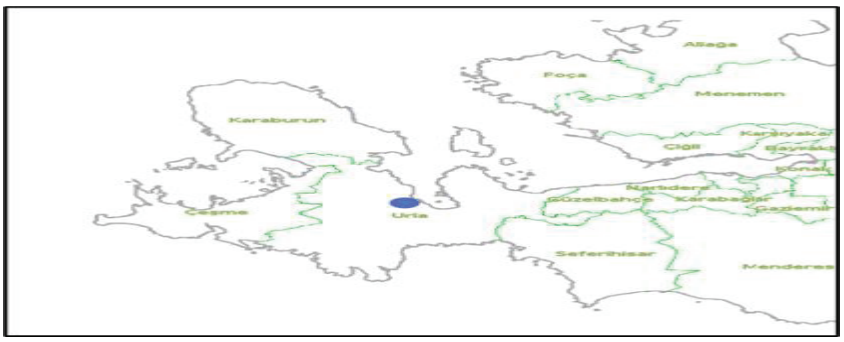

Figure 24. Selected location for the design process (Source: AFAD website)

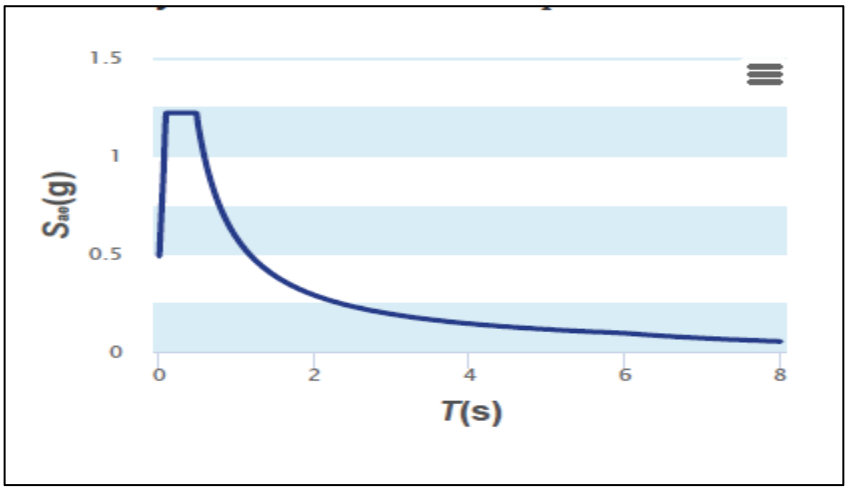

Figure 30. Linear elastic design spectrum for the chosen location (Source: AFAD website)

The live load participation factor has been applied. As recommended by Turkish Earthquake Regulation (TER, 2018), the live load factor is 0.3 for residence type structures. Effective stiffness's of the frame members are defined as given in TER (2018). Reduction factors of 0.7 and 0.35 were applied to the columns and beams respectively.

Most seismic design codes state that under design-level earthquakes, structures should provide the life-safety level. Structural damages are probable in the structures after a design level earthquake. The design-level earthquake is designated as DD2-level in TEC2018 and has a 475-year return period with a 10% chance of exceeding it in 50 years. To evaluate the responses of the frames under such an event, design-level ground motions were applied.

Eleven ground motion records that met the requirements were initially chosen. The chosen ground motion records are scaled such that, in the period range from 0.2T to 1.5T where T is the basic period of the structure, their mean acceleration spectrum does not deviate from the elastic acceleration design spectrum (TEC2018, 2018). Figure 31 displays the elastic design spectrum as well as the individual and mean, mean-plus-one, and mean-minus-one standard deviation spectra of the scaled records.

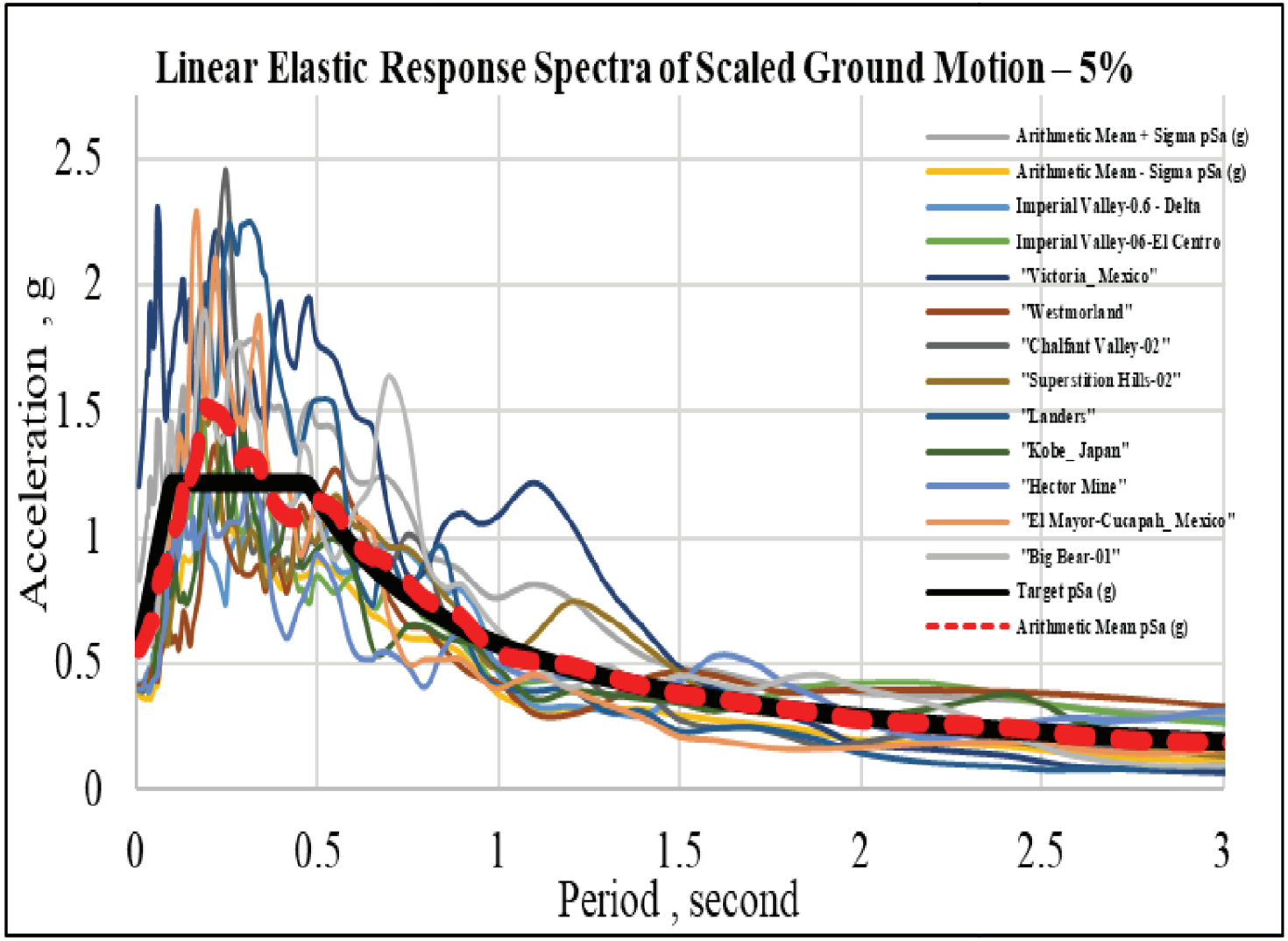

Figure 25. Linear acceleration response spectra of the scaled ground motion records

4.2 Case Study I: Two-Story Three-Bay Frames

Three two-story three-bay frames were designed. Preliminary design of the frames were conducted using TS500 (Turkish Standards, 2003) and later the Turkish Earthquake Regulation (TER 2018) governed the design of the conventional frames mostly the reinforcement detailing. After completing the design procedure, pushover and time-history analysis were performed to the frames using OpenSees (McKenna et al., 2010) platform. Pushover analysis was carried until the hinges occurred in the columns and beams causing frames to turn into mechanism.

4.2.1 Two-Story Three-Bay Frame with SCWB ratio of 1.2-1.5

The first trial is to have a strong-column weak-beam design ratio between 1.2 and 1.5. The member cross-sections and reinforcement were determined to satisfy the selected design ratio. The aim is to monitor the hinges occurrence at the end of members to obtain the failure mechanism and to find the performance levels. For the columns, fiber section is used with two integration points and rotation spring is utilized at the end of each beam. Moment curvature analysis is conducted to calculate the capacity of selected sections for both columns and beams. The capacity of beams are then assigned to the rotation springs to represent the designed beams and these springs are connected to each other by elastic members.

The frames were 2-D moment frames. The exterior bays width are 6.0 meters and the internal bay width is 4.0 meters. For all floors, the story height is 3.0 meters. Figure 32 shows the overview of the frame. The load applied to each floor is 48 KN/m and 12 KN/m for dead and live loads respectively. The mass of each floor is calculated considering these loads. Reinforcement and concrete with characteristic strengths of 420 MPa and 30 MPa were selected for the frames. The members cross-sections and reinforcement details for beams are tabulated in Table 1. The initial period of the frame is 0.42 sec.

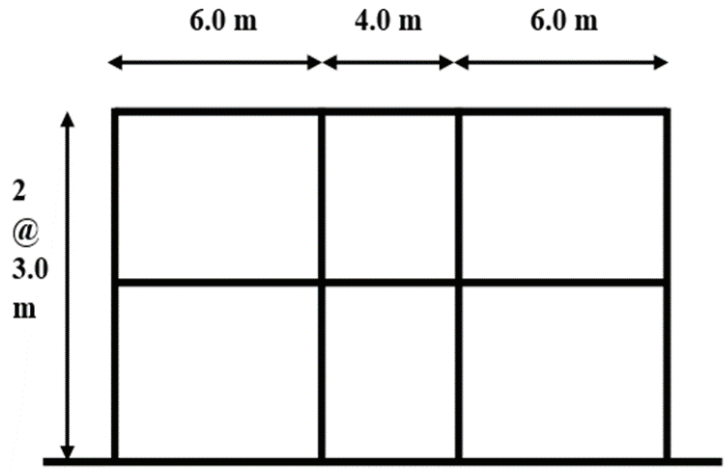

Figure 26. Overview of The two-story two-bay frames

Table 1. Reinforcement and Cross-sections detail of beams for 2-story 3-bay frame, dimensions are in mm.

Story	Location	Inner Bay	Outer Bay	Cross Sectional Size
		Support	Support	
Longitudinal Reinforcement				
1	Top	6Φ14	6Φ18	300x500
	Bottom	3Φ14	3Φ18	
2	Top	6Φ14	6Φ18	
	Bottom	3Φ14	3Φ18	
Transverse Reinforcement				
1	2 legs	Φ10/100	Φ10/100	
2	2 legs	Φ10/100	Φ10/100	

For both columns and beams Equation 5.1 was utilized to calculate the design forces and while designing the columns, the critical condition is taken into account. To prevent the shear failure of the members, TER (2018) defines the minimum requirement for transverse reinforcement. In addition, it provides some checks and procedure to overcome the brittle failure of the members. A spreadsheet was created to check these recommended requirements. The interaction diagram of columns were constructed using the spread sheet created by Ersoy et al (2000).

Table 2 shows the details for reinforcement and cross-sections of the columns for different stories.

Table 2. Cross sections for internal and external columns with reinforcement details. All dimensions are in mm.

Story	Longitudinal Reinforcement		Transverse Reinforcements				Cross Sectional Size	
			Inner		Outer			
	Inner	Outer	Confined Region	Unconfined Region	Confined Region	Unconfined Region	Inner	Outer
1	8Φ22	8Φ18	Φ8/100	Φ8/150	Φ12/90	Φ12/120	400x400	300x400
2	8Φ22	8Φ18	Φ8/100	Φ8/150	Φ12/90	Φ12/120	400x400	300x400

Joint labels of the frame is presented in Figure 33. The force is applied to the frame from left to right. The column-beam design ratios were calculated using the moment capacity of each member and presented in Table 3. It can be seen that the design ratios are in the selected ranges except for the joints at the external joints.

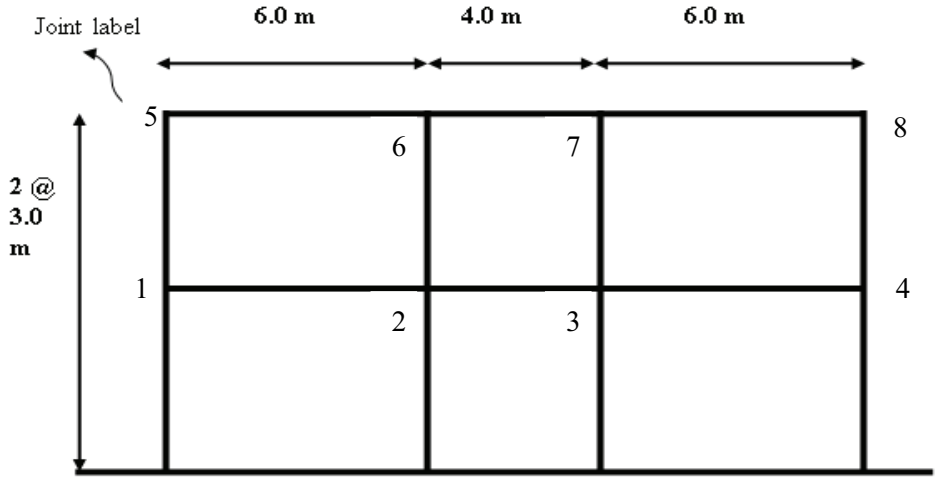

Figure 27. joints' labels of the frame

Table 3. Column-to beam flexural strength ratios of joints

Joints	Column-to-beam strength ratios, β
1	2.24(1)
2	1.29
3	1.5
4	1.2(1)
5	1.04(1)
6	0.61(1)
7	0.71(1)
8	0.54(1)

Notes:
(1) This value may exceed the selected design ratio range because the joint is at the corner.

4.2.1.1 Pushover Analyses

The frame was subjected to the pushover analysis to monitor the occurrence of plastic hinges in the members. The pushover analysis is conducted in OpenSees platform. Capacity curve is used to illustrate the result of the nonlinear static analysis. Figure 34 shows the capacity curve and performance level of the frame.

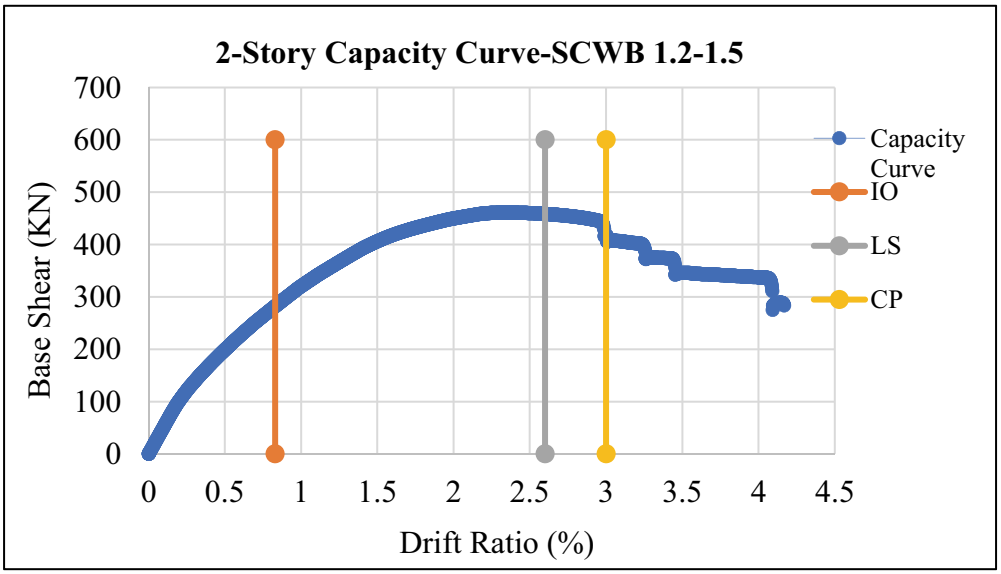

Figure 28. Capacity curve and performance level of the frame

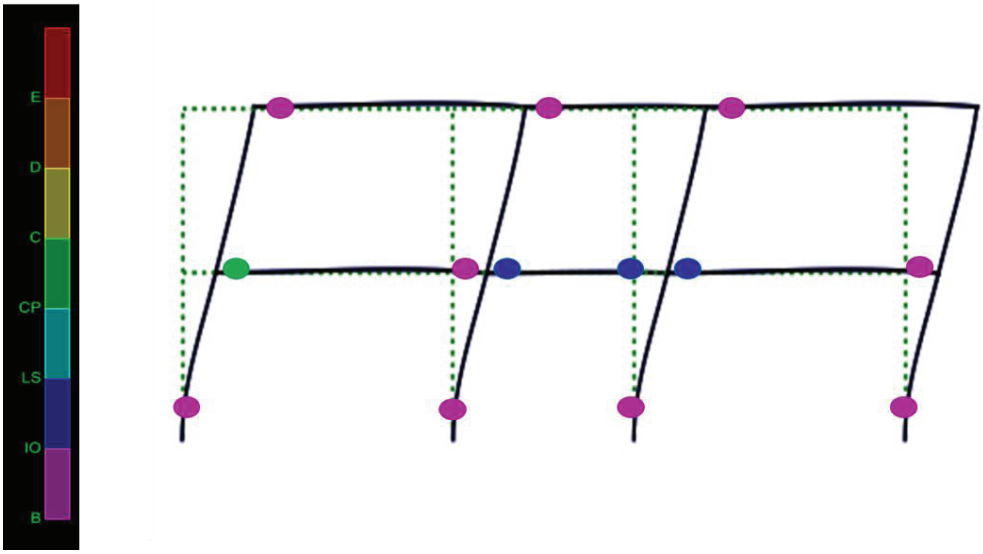

Figure 29. Sway mechanism of the frame obtained from static nonlinear analysis

It can be seen from the figure 35 that the beam hinge mechanism dominates the frame's failure mechanism as expected from the members moments' capacity. The performance level of each elements are shown.

4.2.1.2 Time-History Analyses

The frame was subjected to selected ground motion records to monitor the plastic hinge occurrence in the members. As it is seen in Figure 36, almost the full mechanism has been achieved. The members' flexural design ratio follows the Table 3. Figure 36 shows the rotation variation in the frame obtained through time history analysis.

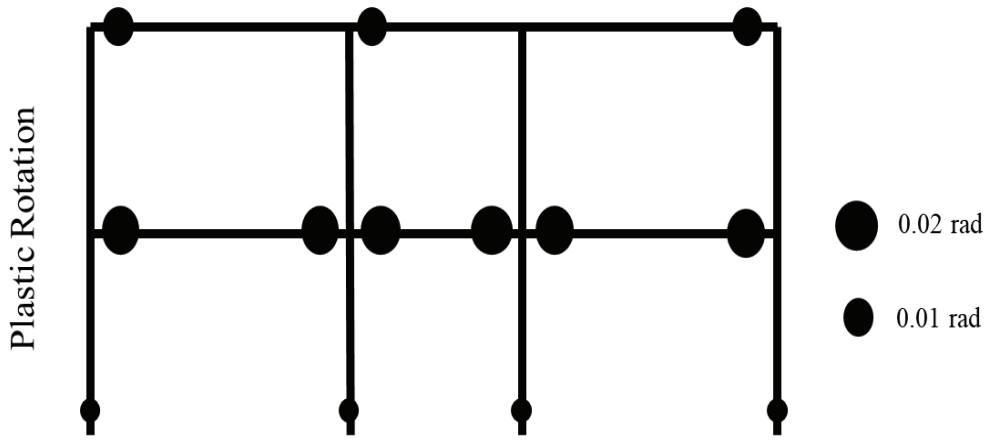

Figure 30. rotation of each element obtained through time history analysis

4.2.2 Two-Story Three-Bay Frame with SCWB ratio of 1.5-2.0

The analyze and design procedures of this frame is the same as the previous one. The only difference is the strong-column weak-beam design ratio which ranges between 1.5 to 2.0. The other parameters and properties are similar with the previous frame. The initial period of the frame is 0.4 sec. The cross-sections and reinforcements details of columns and beams are provided in 4 and 5 respectively. The SCWB ratio of each joint is presented in Table 6. The joints label configuration can be obtained from Figure 33.

Table 4. Cross sections for internal and external columns with reinforcement details. All dimensions are in mm.

Story	Longitudinal Reinforcement		Transverse Reinforcements				Cross Sectional Size	
			Inner		Outer			
	Inner	Outer	Confined Region	Unconfined Region	Confined Region	Unconfined Region	Inner	Outer
1	8Φ24	8Φ18	Φ8/100	Φ8/150	Φ12/90	Φ12/120	400x400	300x400
2	8Φ24	8Φ18	Φ8/100	Φ8/150	Φ12/90	Φ12/120	400x400	300x400

Table 5. Reinforcement and Cross-sections detail of beams for 2-story 3-bay frame, dimensions are in mm.

Story	Location	Inner Bay	Outer Bay	Cross Sectional Size
		Support	Support	
Longitudinal Reinforcement				
1	Top	6Φ14	6Φ18	300x500
	Bottom	3Φ14	3Φ18	
2	Top	6Φ14	6Φ18	
	Bottom	3Φ14	3Φ18	
Transverse Reinforcement				
1	2 legs	Φ10/100	Φ10/100	
2	2 legs	Φ10/100	Φ10/100	

Table 6. Column-to beam flexural strength ratios of joints

Joints	Column-to-beam strength ratios, β
1	2.24(1)
2	1.56
3	1.83
4	1.2(1)
5	1.04(1)
6	0.74(1)
7	0.86(1)
8	0.54(1)

Notes:
(1) This value may exceed the selected design ratio range because the joint is at the corner.

4.2.2.1 Pushover Analyses

The frame was subjected to the nonlinear static analysis to see the behavior of the frame under selected range. Figure 37 shows the capacity curve of the frame for the selected SCWB range and its corresponding performance levels. The performance level of each elements is presented in Figure 38 and beam hinge mechanism governs the failure type.

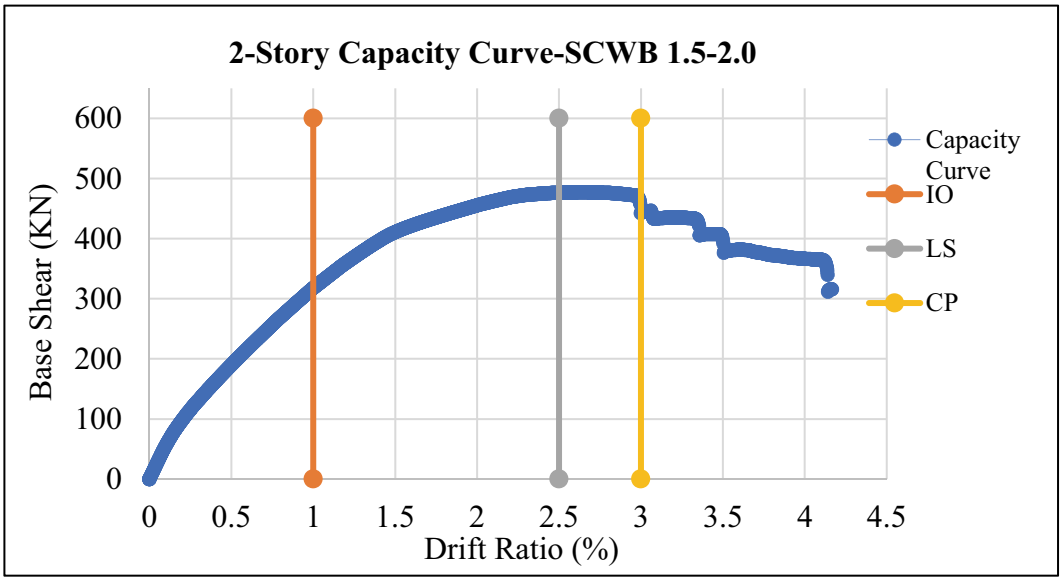

Figure 31. Capacity curve and performance level of the frame

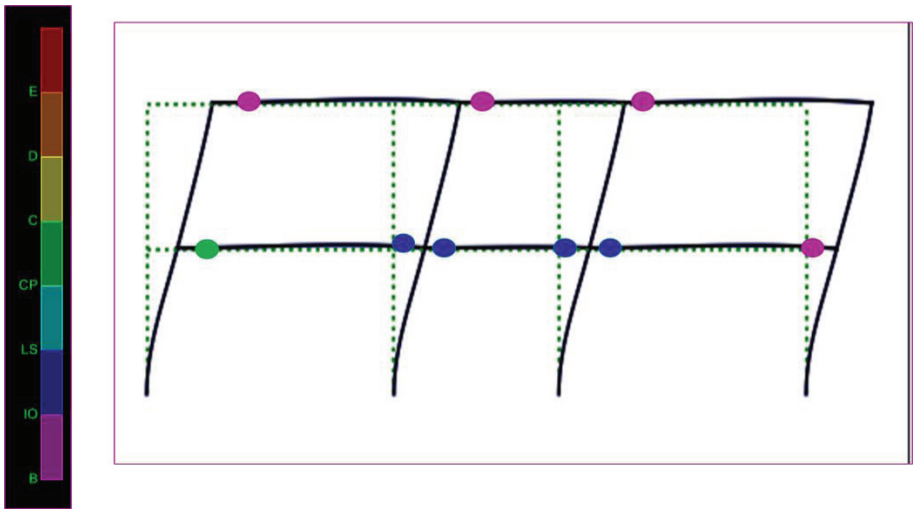

Figure 32. Sway mechanism of the frame obtained from static nonlinear analysis

4.2.2.2 Time-History Analyses

Each member's rotation is obtained through time-history analysis which is shown in Figure 39. The members design ratio follows Table 6. As it can be seen the full hinge mechanism is almost occurred after nonlinear dynamic analysis.

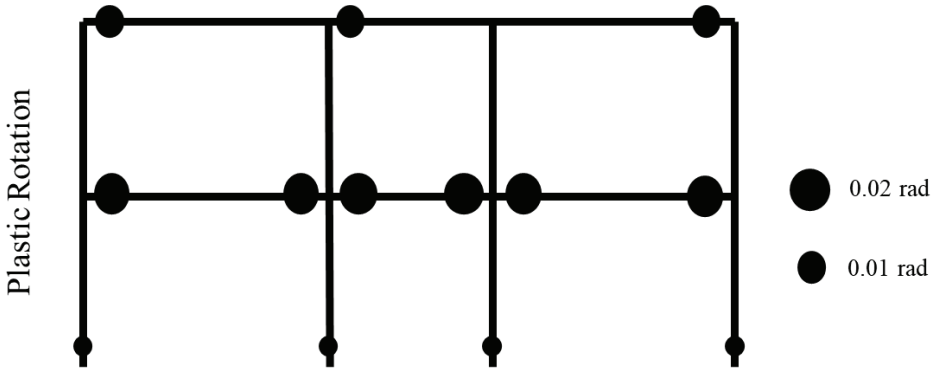

Figure 33. rotation of each element obtained through time history analysis

4.2.3 Two-Story Three-Bay Frame with SCWB ratio of 2.0-3.0

The column-beam design ratio for this case varies between 2.0 and 3.0. This is the last proposed frame for 2-story building. The cross section and reinforcement detail is shown in Table 7 and 8. Other parameters are the same as the previous ones. The SCWB ratio for each joint is presented in Table 9. The joint label numbering can be found from Figure 34. The initial period of the frame is 0.38 sec.

Table 7. Cross sections for internal and external columns with reinforcement details. All dimensions are in mm.

Story	Longitudinal Reinforcement		Transverse Reinforcements				Cross Sectional Size	
			Inner		Outer			
	Inner	Outer	Confined Region	Unconfined Region	Confined Region	Unconfined Region	Inner	Outer
1	8Φ24	8Φ18	Φ8/100	Φ8/150	Φ12/90	Φ12/120	500x500	300x400
2	8Φ24	8Φ18	Φ8/100	Φ8/150	Φ12/90	Φ12/120	500x500	300x400

Table 8. Reinforcement and Cross-sections detail of beams for 2-story 3-bay frame, dimensions are in mm.

Story	Location	Inner Bay	Outer Bay	Cross Sectional Size
		Support	Support	
Longitudinal Reinforcement				
1	Top	6Φ14	6Φ18	300x500
	Bottom	3Φ14	3Φ18	
2	Top	6Φ14	6Φ18	
	Bottom	3Φ14	3Φ18	
Transverse Reinforcement				
1	2 legs	Φ10/100	Φ10/100	
2	2 legs	Φ10/100	Φ10/100	

Table 9. Column-to beam flexural strength ratios of joints

Joints	Column-to-beam strength ratios, β
1	2.24(1)
2	2.1
3	2.5
4	1.2(1)
5	1.04(1)
6	1.0(1)
7	1.14(1)
8	0.54(1)

Notes:
(1) This value may exceed the selected design ratio range because the joint is at the corner.

4.2.3.1 Pushover Analyses

As the previous cases, this frame was also subjected to the pushover analysis to monitor the behavior of the frame. The performance level and capacity curve of the frame are shown in Figure 40. Sway mechanism of the frame along with performance level of each hinge is presented in Figure 41.

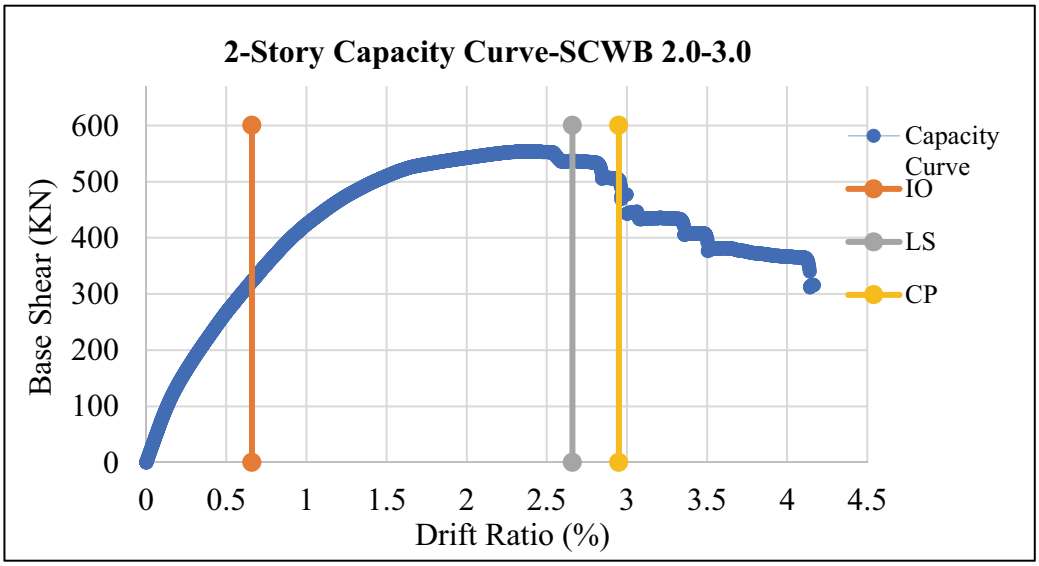

Figure 40. Capacity curve and performance level of the frame

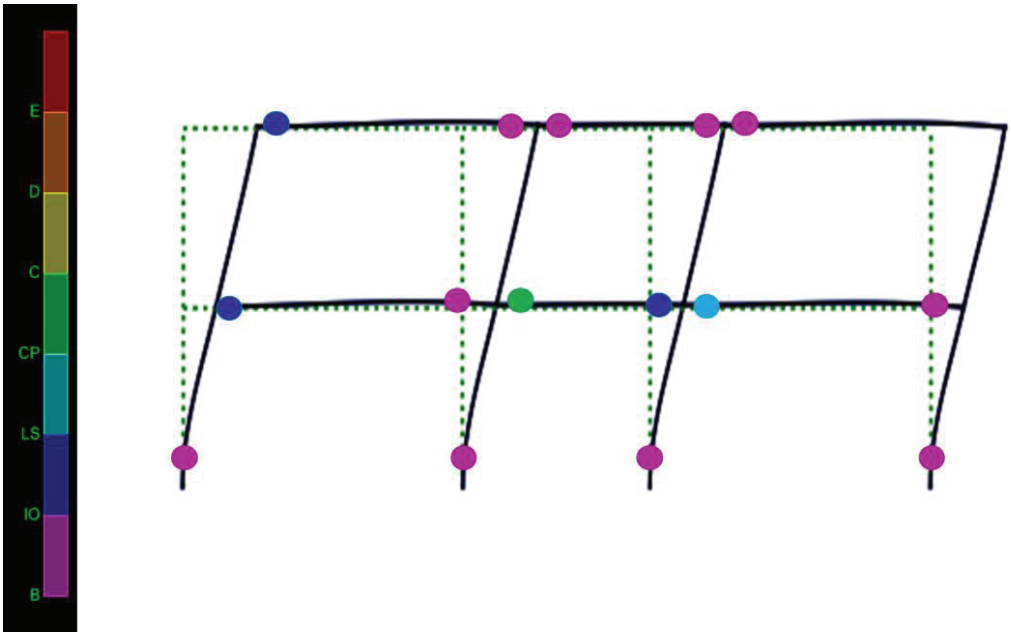

Figure 41. Sway mechanism of the frame obtained from static nonlinear analysis

4.2.3.2 Time-History Analyses

The result of time-history analysis of the frame is shown in Figure 42 as scaled-rotation for each hinge. SCWB ratio is demonstrated in Table 9 for each joint. It is seen that almost full beam hinge mechanism occurs in the system obtained through time-history analysis.

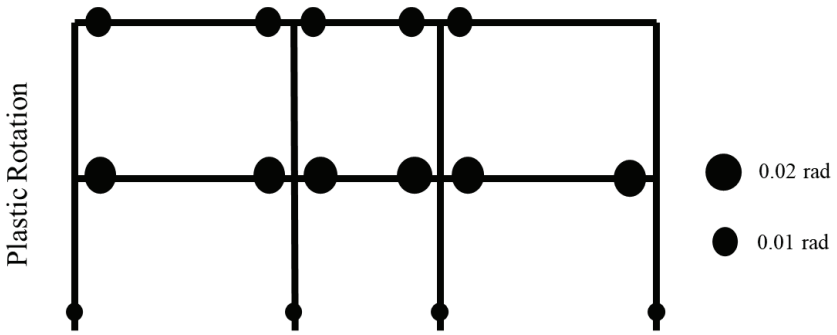

Figure 34. rotation of each element obtained through time history analysis

4.2.4 Discussion of the Results for Two-Story Three-Bays Frames

Three cases were conducted to evaluate the behavior of hinges for different range of SCWB ratio. 1.2 to 1.5, 1.5 to 2.0 and 2.0 to 3.0 SCWB ratio ranges were selected for this purpose. The pushover and time-history analysis were performed to monitor the hinges' performances. The result of the case studies for two-story three-bays frames point out that the different SCWB ratio will not affect the performance level efficiently.

From Figures 34, 37 and 40, it is observed that the performance levels for different levels (Immediate occupancy, Life safety, Collapse prevention) did changed effectively for two story frames. It can be seen from Figures 36, 39 and 42 that the plastic hinges occurrence is a bit enhanced and moved to almost beam hinge mechanism. However, the roof floor does not follow the specified SCWB ratio ranges.

4.3 Case Study II: Five-Story Three-Bay Frames

Three five-story three-bay frames were designed considering the specified SCWB ratios. Turkish Standards 500 (Turkish Standards, 2003) was used for the reference design of the frames. The needed modification is primarily ensured through modifying the reinforcement ratios. Following the design of frames, the OpenSees (McKenna et al., 2010) platform was used to perform pushover and time-history analysis on the frames. Pushover is carried out up until the columns and beams developed hinges, turning the frames into mechanisms.

4.3.1 Five-Story Three-Bay Frame with SCWB ratios of 1.2-1.5

Strong-column weak-beam design ratios between 1.2 and 1.5 are used for the first case. The reinforcement and member cross-sections were obtained to satisfy the chosen design ratio. The goal is to track the formation of hinges at the ends of members in order to identify failure mechanisms and performance levels. The capacity of specific sections for both columns and beams are determined using moment curvature analysis. The rotation springs' capacity comes are obtained for the designed beams Fiber section is utilized for columns containing two integration points.

The frame have the same span geometry. The central bay is 4.0 meters wide, while the external bays are 6.0 meters wide. The story height is 3.0 meters throughout all floors. The overview of the frame and the joints labels are shown in Figure 43. The dead and live loads that are applied to each floor are 48 KN/m and 12 KN/m, respectively. These loads are used to compute the mass of each floor. Same as the two story frames, the material strengths are selected as 420 MPa and 30 MPa for reinforcement and concrete respectively. Table 10 and 11 listed the member geometries and the reinforcement information for columns and beams respectively. The initial period of the system is 0.9 sec.

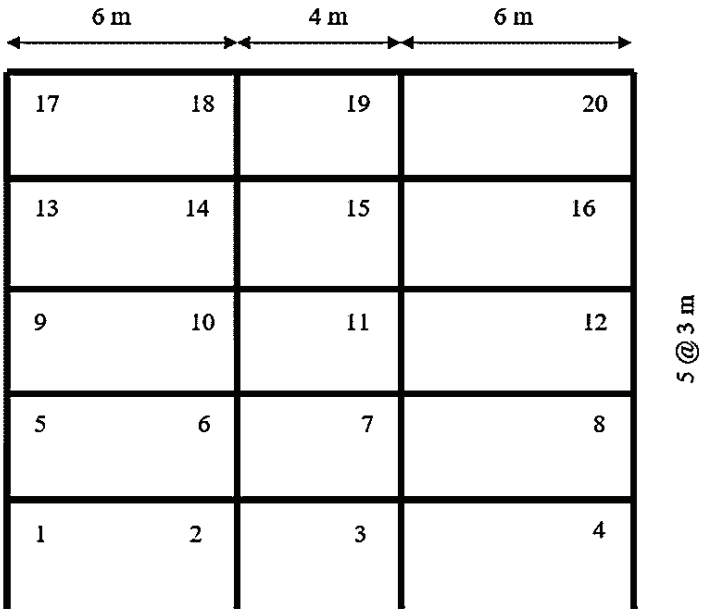

Figure 35. Overview and joints labels of The five-story three-bay frame

Table 10. Cross sections for internal and external columns with reinforcement details. All dimensions are in mm.

Story	Longitudinal Reinforcement		Transverse Reinforcements				Cross Sectional Size	
			Inner		Outer			
	Inner	Outer	Confined Region	Unconfined Region	Confined Region	Unconfined Region	Inner	Outer
1	8Φ22	8Φ22	Φ8/80	Φ8/130	Φ8/100	Φ8/130	500x500	400x400
2	8Φ22	8Φ22	Φ8/80	Φ8/130	Φ8/100	Φ8/130	500x500	400x400
3	8Φ22	8Φ22	Φ8/80	Φ8/130	Φ8/100	Φ8/130	500x500	400x400
4	8Φ22	8Φ18	Φ8/100	Φ8/150	Φ8/100	Φ8/150	400x400	400x400
5	8Φ22	8Φ18	Φ8/100	Φ8/150	Φ8/100	Φ8/150	400x400	400x400

Table 11. Reinforcement and Cross-sections detail of beams, dimensions are in mm.

Story	Location	Inner Bay	Outer Bay	Cross Sectional Size
		Support	Support	
Longitudinal Reinforcement				
1	Top	6Φ20	6Φ20	350x600
	Bottom	3Φ20	3Φ20	
2	Top	6Φ20	6Φ20	
	Bottom	3Φ20	3Φ20	
3	Top	6Φ20	6Φ20	300x500
	Bottom	3Φ20	3Φ20	
4	Top	6Φ14	6Φ20	
	Bottom	3Φ14	3Φ20	
5	Top	6Φ14	6Φ20	
	Bottom	3Φ14	3Φ20	
Transverse Reinforcement				
1	2 legs	Φ8/80	Φ10/110	350x600
2	2 legs	Φ8/80	Φ10/110	
3	2 legs	Φ10/90	Φ10/90	300x500
4	2 legs	Φ8/100	Φ10/90	
5	2 legs	Φ8/100	Φ10/90	

Table 12. Column-to beam flexural strength ratios of joints for SCWB 1.2-1.5

Joints	Column-to-beam strength ratios, β
1	2.66(1)
2	1.37
3	1.44
4	1.39(1)
5	2.54(1)
6	1.28
7	1.35
8	1.34(1)
9	2.53(1)
10	1.44
11	1.5
12	1.64(1)
13	1.93(1)
14	1.36
15	1.48
16	1.23(1)
17	0.9(1)
18	0.63(1)
19	0.68(1)
20	0.57(1)

Notes:
(1) This value may exceed the selected design ratio range because the joint is at the corner.

4.3.1.1 Pushover Analyses

The OpenSees platform is used to carry out the pushover analysis. An illustration of the outcome of the nonlinear static analysis is shown as the capacity curve. The capacity curve and performance level of the frame are displayed in Figure 44. The sway mechanism of the frame is presented in Figure 45.

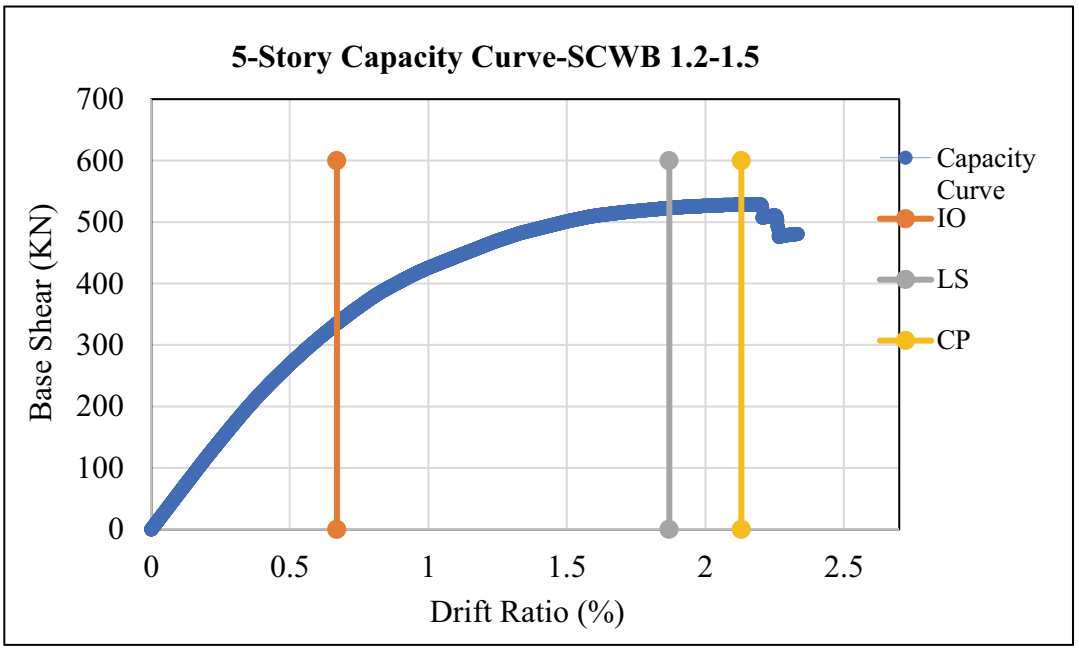

Figure 36. Capacity curve and performance level of 5-Story frame for SCWB of 1.2 up to 1.5

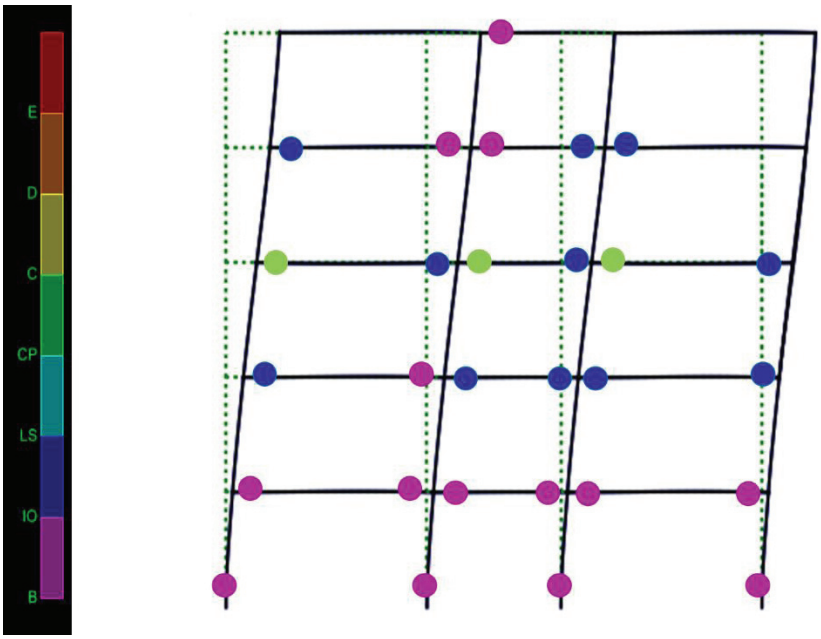

Figure 37. Sway mechanism of the frame obtained from static nonlinear analysis for SCWB of 1.2 up to 1.5

4.3.1.2 Time-History Analyses

Plastic hinge rotations for each hinge formed in the frame for time history analysis are presented in in Figure 46. These rotations show the average of the absolute value maximums occurred in the system through nonlinear dynamic analysis. The hinge sizes are scaled according the magnitudes of rotations. The reference hinge rotations are shown at the right of the figure.

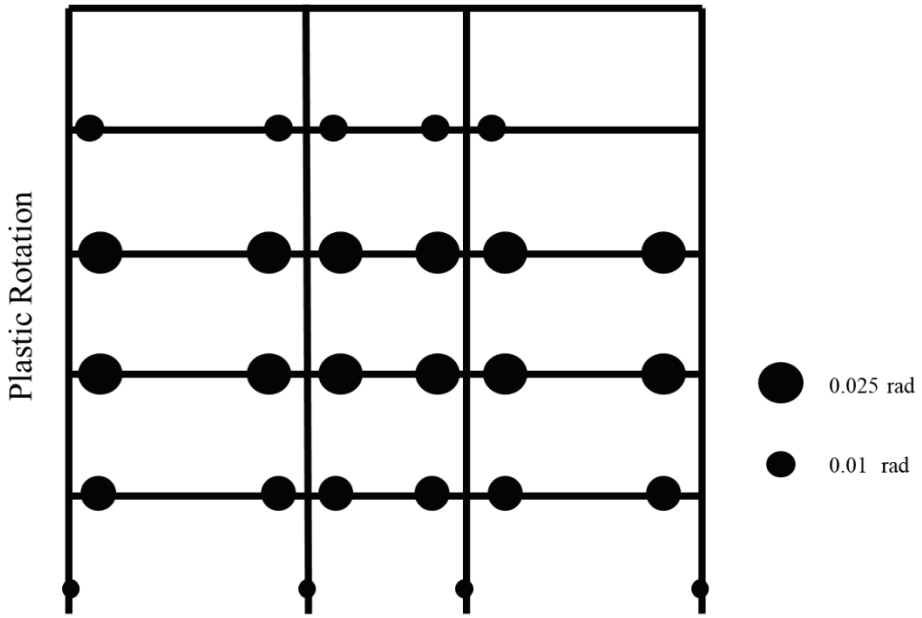

Figure 38. rotation of each element obtained through time history analysis for SCWB of 1.2 up to 1.5

4.3.2 Five-Story Three-Bay Frame with SCWB ratio of 1.5-2.0

The second trial for this case was to change the SCWB range from 1.5 up to 2.0. All other parameters and procedures are the same as the first frame. The reinforcement and cross sectional details of the system can be found from Table 13 and 14. The SCWB ratio for each joint is presented in Table 16 for this case. The initial period is 0.85 sec for the frame.

Table 13. Cross sections for internal and external columns with reinforcement details. All dimensions are in mm.

Story	Longitudinal Reinforcement		Transverse Reinforcements				Cross Sectional Size	
			Inner		Outer			
	Inner	Outer	Confined	Unconfined Region	Confined Region	Unconfined Region	Inner	Outer
1	8Φ22	8Φ22	Φ8/80	Φ8/130	Φ8/100	Φ8/130	500x500	400x400
2	8Φ22	8Φ22	Φ8/80	Φ8/130	Φ8/100	Φ8/130	500x500	400x400
3	8Φ22	8Φ22	Φ8/80	Φ8/130	Φ8/100	Φ8/130	500x500	400x400
4	8Φ24	8Φ18	Φ8/100	Φ8/150	Φ8/100	Φ8/150	400x400	400x400
5	8Φ24	8Φ18	Φ8/100	Φ8/150	Φ8/100	Φ8/150	400x400	400x400

Table 14. Reinforcement and Cross-sections detail of beams, dimensions are in mm.

Story	Location	Inner Bay	Outer Bay	Cross Sectional Size
		Support	Support	
Longitudinal Reinforcement				
1	Top	6Φ18	6Φ18	350x600
	Bottom	3Φ18	3Φ18	
2	Top	6Φ18	6Φ18	
	Bottom	3Φ18	3Φ18	
3	Top	6Φ18	6Φ18	
	Bottom	3Φ18	3Φ18	
4	Top	6Φ14	6Φ20	300x500
	Bottom	3Φ14	3Φ20	
5	Top	6Φ14	6Φ20	
	Bottom	3Φ14	3Φ20	
Transverse Reinforcement				
1	2 legs	Φ8/80	Φ10/110	350x600
2	2 legs	Φ8/80	Φ10/110	
3	2 legs	Φ10/90	Φ10/90	
4	2 legs	Φ8/100	Φ10/90	300x500
5	2 legs	Φ8/100	Φ10/90	

Table 15. Column-to beam flexural strength ratios of joints for SCWB 1.5-2.0

Joints	Column-to-beam strength ratios, β
1	3.27(1)
2	1.74
3	1.84
4	1.74(1)
5	3.13(1)
6	1.63
7	1.73
8	1.68(1)
9	2.55(1)
10	1.65
11	2.0
12	1.37(1)
13	1.93(1)
14	1.57
15	1.7
16	1.23(1)
17	0.9(1)
18	0.74(1)
19	0.8(1)
20	0.57(1)

Notes:
(1) This value may exceed the selected design ratio range because the joint is at the corner.

4.3.2.1 Pushover Analyses

The frame was subjected to a pushover analysis to determine plastic hinges and their corresponding performance level as shown in Figure 47. The capacity curve serves as an example of the results of the nonlinear static analysis (see Figure 48).

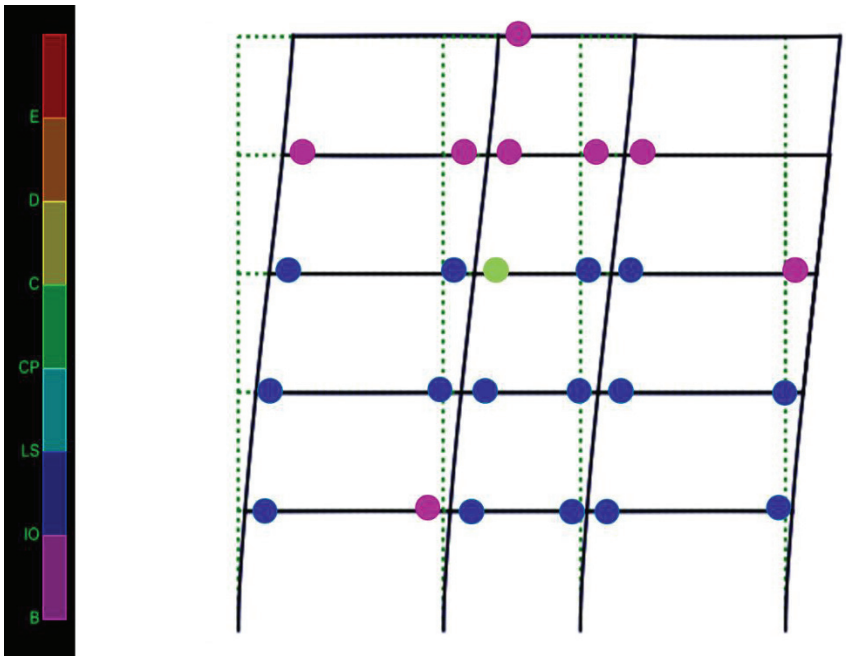

Figure 39. Sway mechanism of the frame obtained from static nonlinear analysis for SCWB of 1.5 up to 2.0

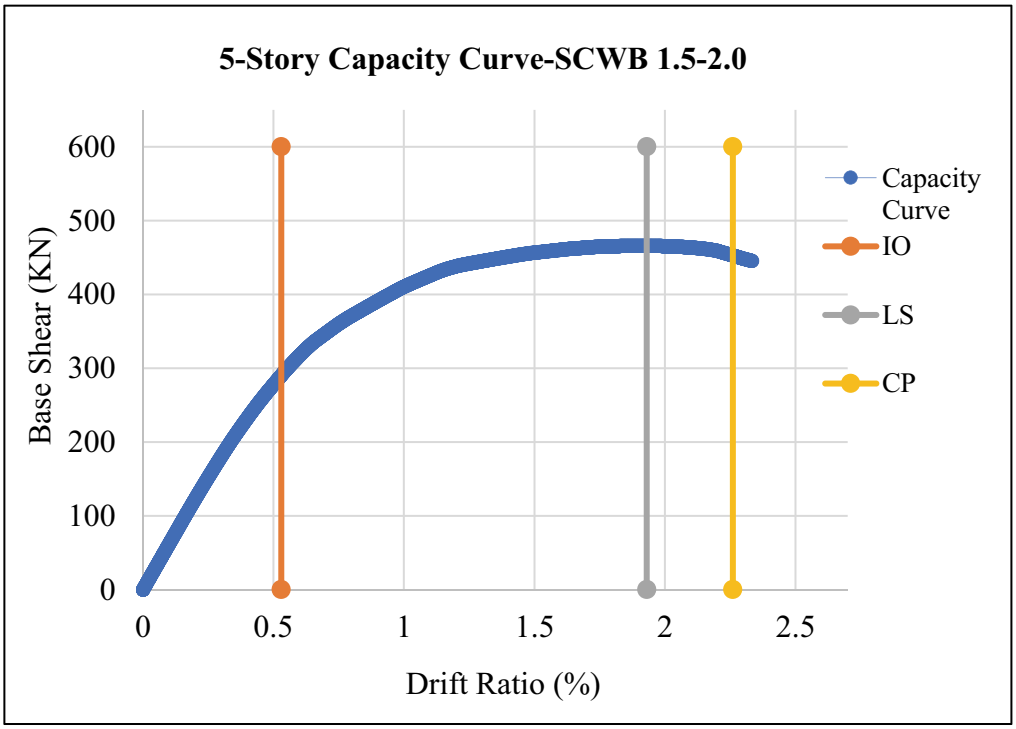

Figure 40. Capacity curve and performance level of 5-Story frame for SCWB of 1.5 up to 2.0

4.3.2.2 Time-History Analyses

The result of the time-history analysis of the frame, as shown in Figure 49, is a scaled-rotation for each hinge. These rotations demonstrates the average of the absolute value maximums of the hinge rotations for the nonlinear time history analysis of frame.

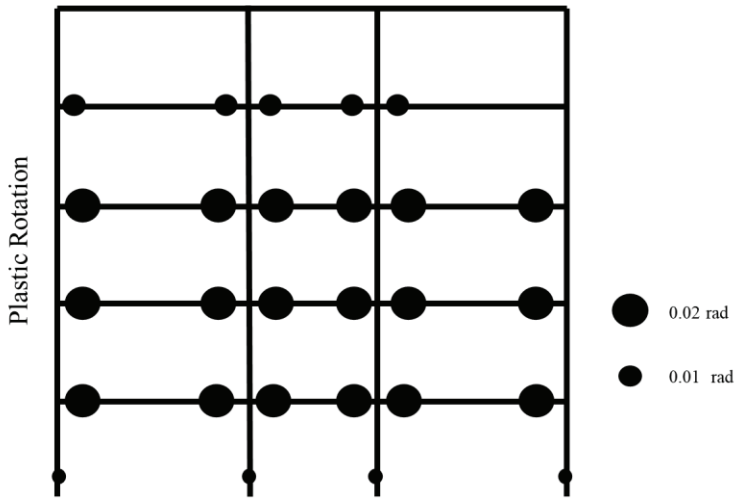

Figure 41. rotation of each element obtained through time history analysis for SCWB of 1.5 up to 2.0

4.3.3 Five-Story Three-Bay Frame with SCWB ratio of 2.0-3.0

The third trial for this case is to use SCWB ratio of 2.0 up to 3.0. The other parameters and procedures are unchanged. Tables 16 and 17 contain information on the system's reinforcement and cross-sectional details of columns and beams. Table 18 for this trail shows the SCWB ratio for each joint following Figure 43 labels. The initial period for this frame was 0.82 sec.

Table 16. Cross sections for internal and external columns with reinforcement details. All dimensions are in mm.

Story	Longitudinal Reinforcement		Transverse Reinforcements				Cross Sectional Size	
			Inner		Outer			
	Inner	Outer	Confined Region	Unconfined Region	Confined Region	Unconfined Region	Inner	Outer
1	8Φ26	8Φ22	Φ10/100	Φ10/130	Φ8/100	Φ8/130	500x500	400x400
2	8Φ26	8Φ22	Φ10/100	Φ10/130	Φ8/100	Φ8/130	500x500	400x400
3	8Φ26	8Φ22	Φ10/100	Φ10/130	Φ8/100	Φ8/130	500x500	400x400
4	8Φ24	8Φ18	Φ8/100	Φ8/150	Φ8/100	Φ8/150	500x500	400x400
5	8Φ24	8Φ18	Φ8/100	Φ8/150	Φ8/100	Φ8/150	500x500	400x400

Table 17. Reinforcement and Cross-sections detail of beams, dimensions are in mm.

Story	Location	Inner Bay	Outer Bay	Cross Sectional Size	
		Support	Support		
Longitudinal Reinforcement				Inner	Outer
1	Top	6Φ20	6Φ18	300x500	350x600
	Bottom	3Φ20	3Φ18		
2	Top	6Φ20	6Φ18		
	Bottom	3Φ20	3Φ18		
3	Top	6Φ20	6Φ18		
	Bottom	3Φ20	3Φ18		
4	Top	6Φ14	6Φ18	300x500	
	Bottom	3Φ14	3Φ18		
5	Top	6Φ14	6Φ18		
	Bottom	3Φ14	3Φ18		
Transverse Reinforcement					
1	2 legs	Φ8/80	Φ10/110	300x500	350x600
2	2 legs	Φ8/80	Φ10/110		
3	2 legs	Φ10/90	Φ10/90		
4	2 legs	Φ8/100	Φ10/90	300x500	
5	2 legs	Φ8/100	Φ10/90		

Table 18. Column-to beam flexural strength ratios of joints for SCWB 2.0-3.0

Joints	Column-to-beam strength ratios, β
1	3.27(1)
2	2.12
3	2.46
4	1.74(1)
5	3.13(1)
6	2.03
7	2.36
8	1.68(1)
9	2.55(1)
10	2.14
11	2.71
12	1.37(1)
13	1.93(1)
14	2.07
15	2.25
16	1.23(1)
17	0.9(1)
18	0.97(1)
19	1.04(1)
20	0.57(1)

4.3.3.1 Pushover Analyses

Figure 49 displays the outcome of the frame's nonlinear static analysis. These results include the frame's performance level and capacity curve. Figure 50 also illustrates the specific performance level of each spring.

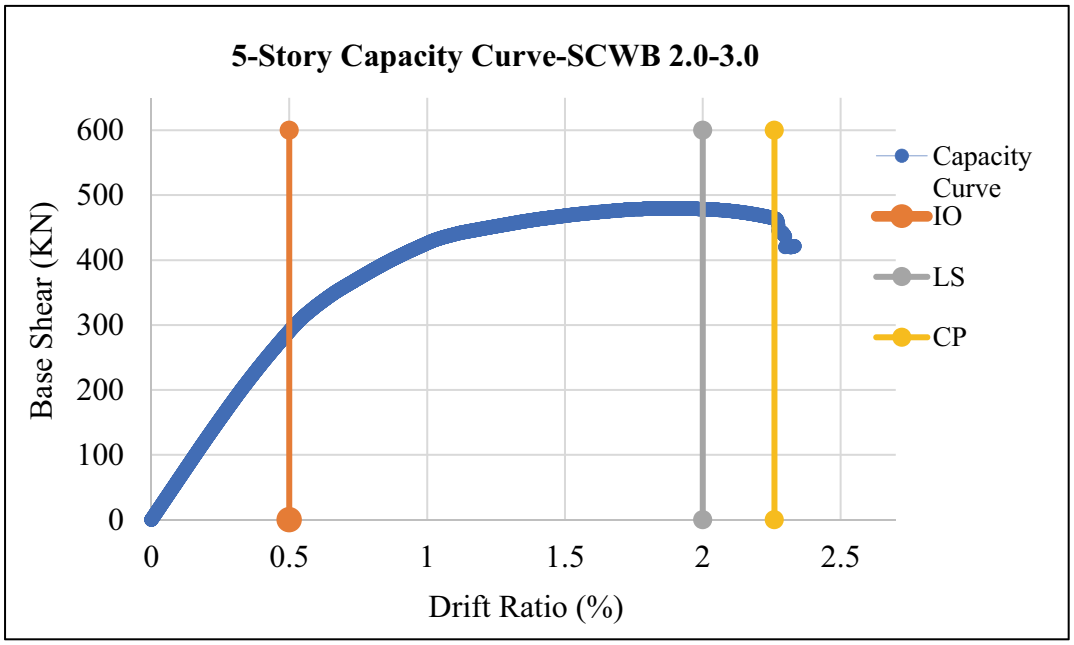

Figure 42. Capacity Curve and Performance Level of the Frame (SCWB 2.0-3.0)

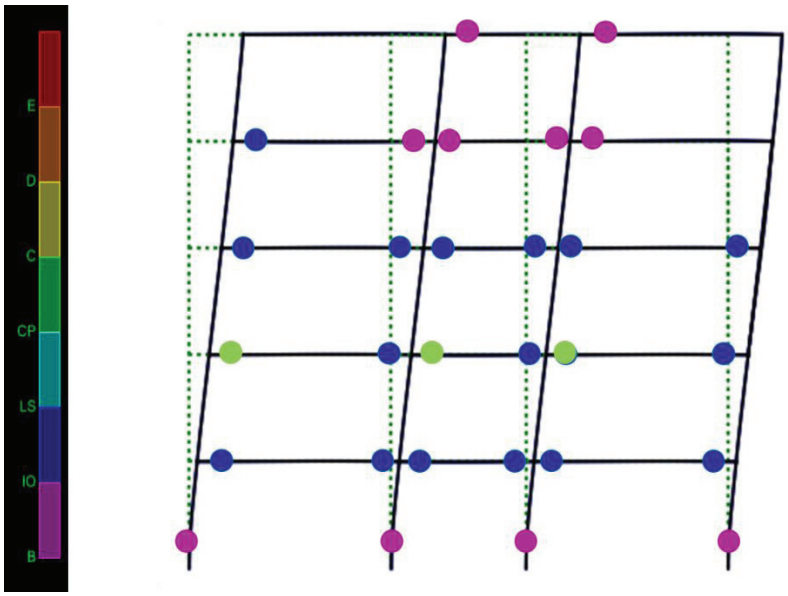

Figure 43. Sway mechanism of the frame obtained from static nonlinear analysis for SCWB of 2.0 up to 3.0

4.3.3.2 Time-History Analyses

A scaled-rotation for each hinge is the outcome of the time-history study of the frame, as shown in Figure 51. These rotations show how nonlinear dynamic analysis identified the maximum and minimum impacts of the system.

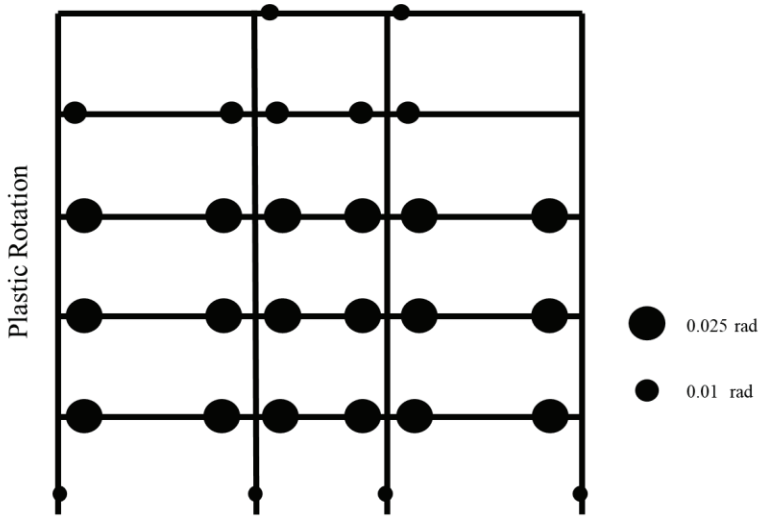

Figure 44. rotation of each element obtained through time history analysis for SCWB of 2.0 up to 3.0

4.3.4 Discussion of the Results for Five-Story Three-Bays Frames

As the SCWB increases, there is a slight improvement in the behavior, as shown by the capacity curves and performance levels of all three frames. Performance levels improve as the location between IO (Immediate Occupancy) and LS (Life Safety) distance increases. In addition, as SCWB increases, more beams are engaged in the failure mechanism, as shown in Figure 50 when compared to the outcomes of earlier cases. This minor advancement is also visible in Figure 51, where scaled-rotation depicts a greater number of beams exceeding the yield capacity.

4.4 Case Study III: Eight-Story Three-Bay Frames

Three eight-story three-bay models were created while taking into account the required SCWB ratio. Initial frame design was based on Turkish Requirements (Turkish Standards, 2003). Later, the reinforcing detailing of the conventional frames was guided by the Turkish Earthquake Regulation (TER 2018). Following the design phase, pushover and time-history analysis on the frames were carried out using the OpenSees (McKenna et al., 2010) framework. This study was conducted until the beams and columns began to develop hinges, which turned the frames into mechanisms.

4.4.1 Eight-Story Three-Bay Frame with SCWB ratio of 1.2-1.5

For the first trial, design ratios of strong-column weak-beams between 1.2 and 1.5 are employed. To meet the selected design ratio, the reinforcement and member cross-sections were obtained. The objective is to monitor the occurrence of hinges at the extremities of members in order to determine failure mechanisms and performance levels. Moment curvature analysis is used to measure the strength of particular sections for both columns and beams. The capacity of the rotation springs is provided by designed frames, and they are connected to one another by elastic elements. For columns with two integration points, fiber section is used.

The external bays are 6.0 meters wide, compared to 4.0 meters for the center bay. The story height is 3.0 meters throughout all levels. Figure 52 displays the frame's overall layout as well as the markings for the joints. Each level is subjected to 48 KN/m in dead loads and 12 KN/m in live loads. The masses of each level are calculated using these loads. Similar to other cases material characteristics strengths of 30.0 MPa and 420 MPa were selected for concrete and steel respectively. The cross-sections of the components and the reinforcing details for columns and beams are listed in Tables 19 and 20 respectively. SCWB ratio of the frame is shown in Table 21. The initial period of the system is 1.04 sec.

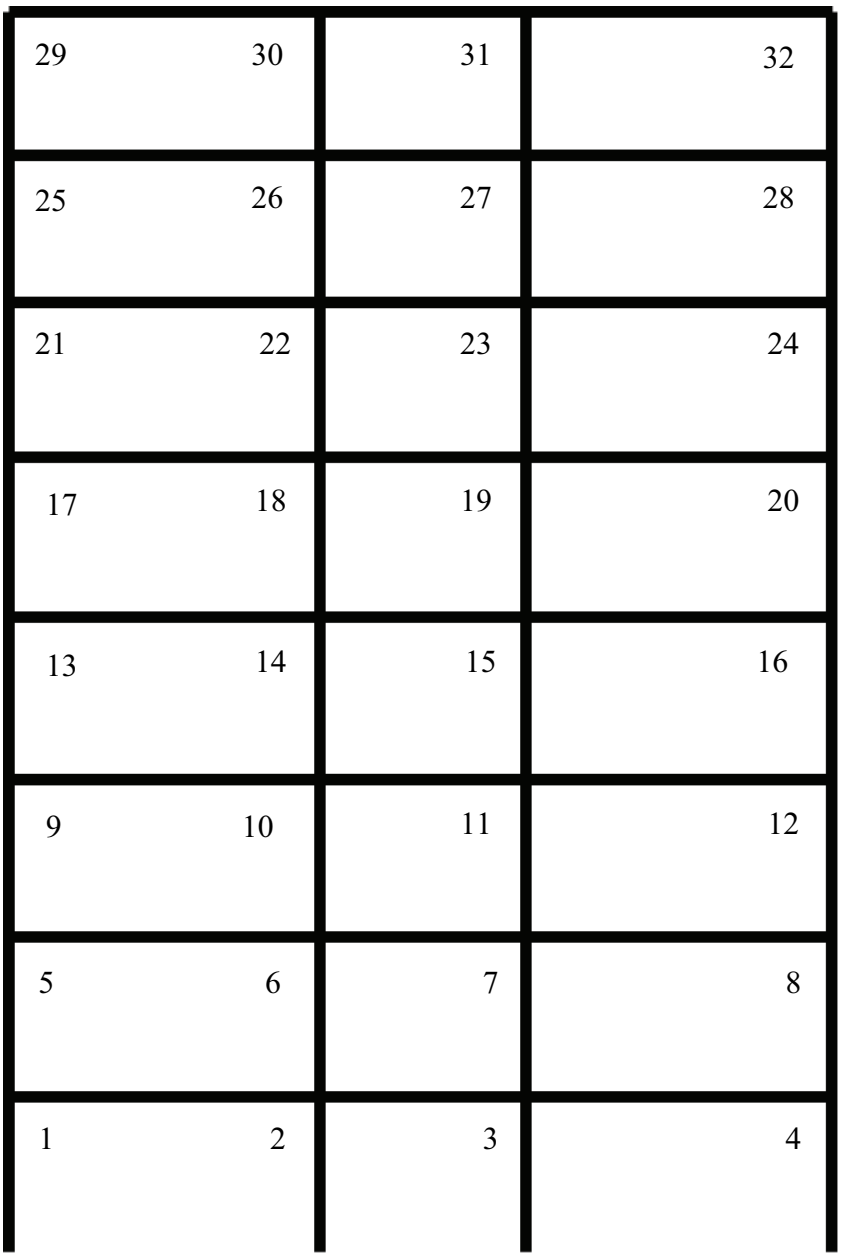

Figure 45. Frame's overall layout as well as the markings for the joints

Table 19. Cross sections for internal and external columns with reinforcement details. All dimensions are in mm.

Story	Longitudinal Reinforcement		Transverse Reinforcements				Cross Sectional Size	
			Inner		Outer			
	Inner	Outer	Confined Region	Unconfined Region	Confined Region	Unconfined Region	Inner	Outer
1	12Φ18	12Φ22	Φ10/70	Φ10/120	Φ8/100	Φ8/130	500x600	500x500
2	12Φ18	12Φ22	Φ10/70	Φ10/120	Φ8/100	Φ8/130	500x600	500x500
3	12Φ18	12Φ22	Φ10/70	Φ10/120	Φ8/100	Φ8/130	500x600	500x500
4	12Φ18	12Φ22	Φ10/70	Φ10/120	Φ8/100	Φ8/130	500x600	500x500
5	12Φ18	12Φ22	Φ10/70	Φ10/120	Φ8/100	Φ8/130	500x600	500x500
6	12Φ16	12Φ16	Φ8/130	Φ8/150	Φ8/130	Φ8/150	500x500	500x500
7	12Φ16	12Φ16	Φ8/130	Φ8/150	Φ8/130	Φ8/150	500x500	500x500
8	12Φ16	12Φ16	Φ8/130	Φ8/150	Φ8/130	Φ8/150	500x500	500x500

Table 20. Reinforcement and Cross-sections detail of beams, dimensions are in mm.

Story	Location	Inner Bay	Outer Bay	Cross Sectional Size	
		Support	Support		
Longitudinal Reinforcement				Inner	Outer
1	Top	6Φ22	6Φ22	350x600	
	Bottom	3Φ22	3Φ22		
2	Top	6Φ22	6Φ22		
	Bottom	3Φ22	3Φ22		
3	Top	6Φ22	6Φ22		
	Bottom	3Φ22	3Φ22		
4	Top	6Φ22	6Φ22		
	Bottom	3Φ22	3Φ22		
5	Top	6Φ18	6Φ20		

	Bottom	3Φ18	3Φ20	
6	Top	6Φ18	6Φ18	
	Bottom	3Φ18	3Φ18	
7	Top	6Φ18	6Φ18	
	Bottom	3Φ18	3Φ18	
8	Top	6Φ18	6Φ18	
	Bottom	3Φ18	3Φ18	
Transverse Reinforcement				
1	2 legs	Φ10/100	Φ10/100	350x600
2	2 legs	Φ10/100	Φ10/100	
3	2 legs	Φ10/100	Φ10/100	
4	2 legs	Φ10/100	Φ10/100	
5	2 legs	Φ8/150	Φ10/110	
6	2 legs	Φ8/150	Φ8/150	
7	2 legs	Φ8/150	Φ8/150	
8	2 legs	Φ8/150	Φ8/150	

Table 21. Column-to beam flexural strength ratios of joints for SCWB 1.2-1.5

Joints	**Column-to-beam strength ratios**
1	3.93(1)
2	1.42
3	1.5
4	2.2(1)
5	3.85(1)
6	1.36
7	1.49
8	2.15(1)
9	3.80(1)
10	1.29
11	1.43
12	2.1(1)
13	3.76(1)
14	1.23
15	1.3
16	2.02(1)
17	3.76(1)
18	1.37
19	1.5
20	1.97(1)
21	3.27(1)
22	1.27
23	1.29
24	1.8(1)
25	2.97(1)
26	1.2
27	1.21
28	1.6(1)
29	1.41(1)
30	0.5(1)
31	0.5(1)
32	0.73(1)

4.4.1.1 Pushover Analyses

To identify the plastic hinges and their associated performance levels, the frame was put through a pushover analysis, as seen in Figure 53. An illustration of the outcomes of each plastic hinges after nonlinear static analysis is shown in Figure 54.

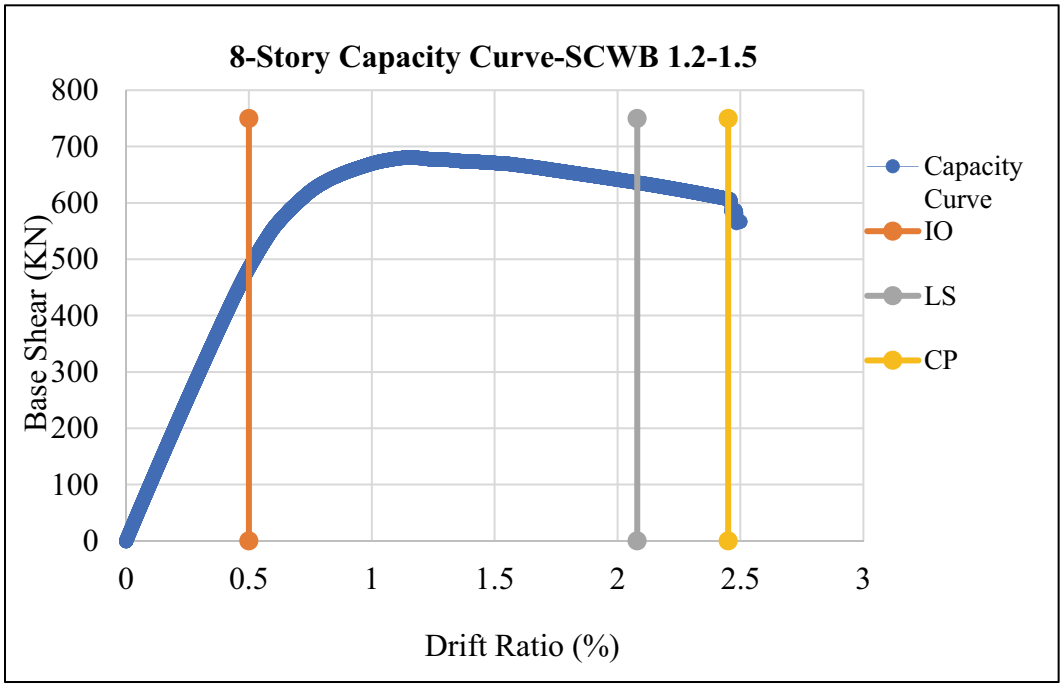

Figure 46. Capacity Curve and Performance Level of the Frame (SCWB: 1.2-1.5)

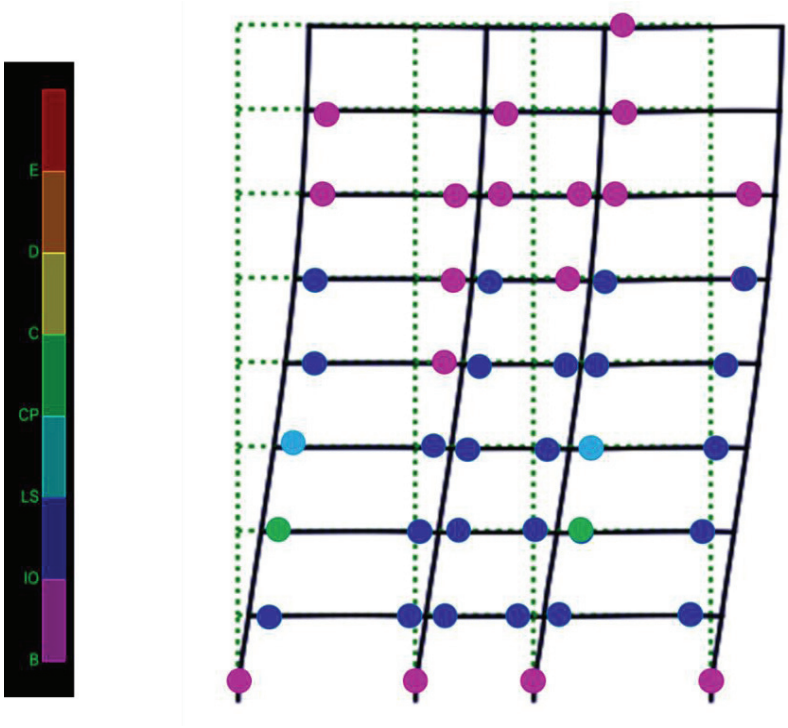

Figure 47. Sway mechanism of the frame obtained from static nonlinear analysis for SCWB of 1.2 up to 1.5

4.4.1.2 Time-History Analyses

The result of the time-history analysis of the frame is a scaled-rotation for each joint, as depicted in Figure 55. These rotations approximates how nonlinear dynamic analysis was able to determine the system's behavior when earthquake occurs.

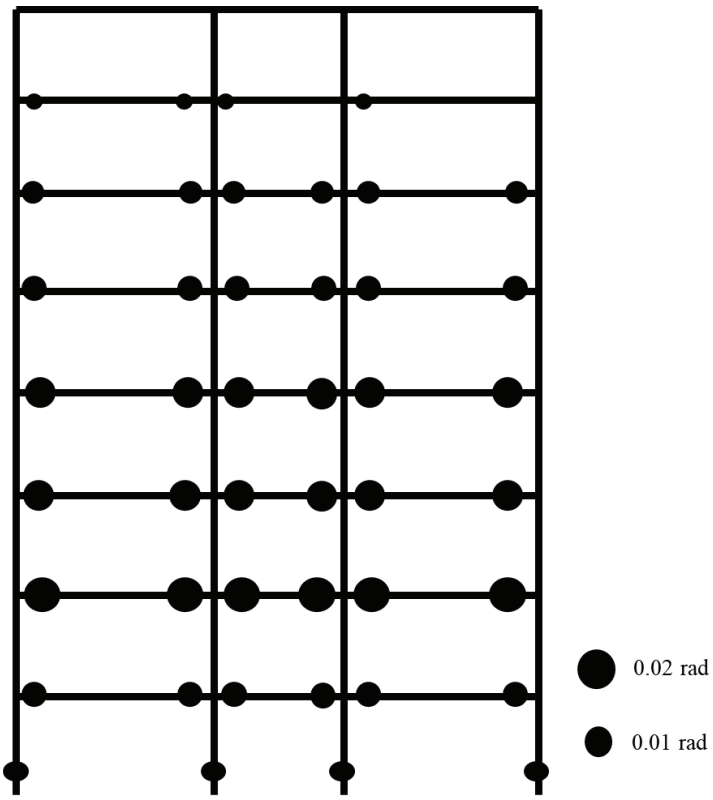

Figure 48. Rotation of each element obtained through time history analysis for SCWB of 1.2 to 1.5

4.4.2 Eight-Story Three-Bay Frame with SCWB ratio of 1.5-2.0

The SCWB range was changed to 1.5 up to 2.0 in the second trial for this instance. The previous one's procedures and other parameters are still in place. Tables 22 and 23 contain information on the system's reinforcement and cross-sectional specifications. Table 24 for this instance shows the SCWB ratio for each joint. The initial period was 1.0 sec.

Table 22. Cross sections for internal and external columns with reinforcement details. All dimensions are in mm.

Story	Longitudinal Reinforcement		Transverse Reinforcements				Cross Sectional Size	
			Inner		Outer			
	Inner	Outer	Confined Region	Unconfined Region	Confined Region	Unconfined Region	Inner	Outer
1	12Φ18	12Φ22	Φ10/70	Φ10/120	Φ8/100	Φ8/130	500x600	500x500
2	12Φ18	12Φ22	Φ10/70	Φ10/120	Φ8/100	Φ8/130	500x600	500x500
3	12Φ18	12Φ22	Φ10/70	Φ10/120	Φ8/100	Φ8/130	500x600	500x500
4	12Φ18	12Φ22	Φ10/70	Φ10/120	Φ8/100	Φ8/130	500x600	500x500
5	12Φ18	12Φ22	Φ10/70	Φ10/120	Φ8/100	Φ8/130	500x600	500x500
6	12Φ16	12Φ16	Φ8/130	Φ8/150	Φ8/130	Φ8/150	500x500	500x500
7	12Φ16	12Φ16	Φ8/130	Φ8/150	Φ8/130	Φ8/150	500x500	500x500
8	12Φ16	12Φ16	Φ8/130	Φ8/150	Φ8/130	Φ8/150	500x500	500x500

Table 23. Reinforcement and Cross-sections detail of beams, dimensions are in mm.

Story	Location	Inner Bay	Outer Bay	Cross Sectional Size	
		Support	Support		
Longitudinal Reinforcement				Inner	Outer
1	Top	6Φ20	6Φ20	350x600	
	Bottom	3Φ20	3Φ20		
2	Top	6Φ20	6Φ20		
	Bottom	3Φ20	3Φ20		
3	Top	6Φ20	6Φ20		
	Bottom	3Φ20	3Φ20		
4	Top	6Φ20	6Φ20		
	Bottom	3Φ20	3Φ20		
5	Top	6Φ20	6Φ20	300x500	
	Bottom	3Φ18	3Φ20		
6	Top	6Φ14	6Φ20		
	Bottom	3Φ14	3Φ20		
7	Top	6Φ14	6Φ20		
	Bottom	3Φ14	3Φ20		
8	Top	6Φ14	6Φ20		
	Bottom	3Φ14	3Φ20		
Transverse Reinforcement					
1	2 legs	Φ10/110	Φ10/110	350x600	
2	2 legs	Φ10/110	Φ10/110		
3	2 legs	Φ10/110	Φ10/110		
4	2 legs	Φ10/110	Φ10/110		
5	2 legs	Φ10/90	Φ10/90	300x500	
6	2 legs	Φ8/100	Φ10/90		
7	2 legs	Φ8/100	Φ10/90		
8	2 legs	Φ8/100	Φ10/90		

Table 24. Column-to beam flexural strength ratios of joints for SCWB 1.5-2.0

Joints	**Column-to-beam strength ratios**
1	4.93(1)
2	1.77
3	1.98
4	2.7(1)
5	4.85(1)
6	1.7
7	1.9
8	2.66(1)
9	4.77(1)
10	1.62
11	1.78
12	2.6(1)
13	4.73(1)
14	1.53
15	1.64
16	2.51(1)
17	4.27(1)
18	1.65
19	1.72
20	2.7(1)
21	3.0(1)
22	1.64
23	1.84
24	1.98(1)
25	2.75(1)
26	1.5
27	1.58
28	1.77(1)
29	1.3(1)
30	0.64(1)
31	0.71(1)
32	0.81(1)

4.4.2.1 Pushover Analyses

The frame underwent a pushover analysis, as depicted in Figure 56, to determine the plastic hinges and the performance levels related with them. Figure 57 illustrates the results of each plastic hinge behavior after nonlinear static analysis.

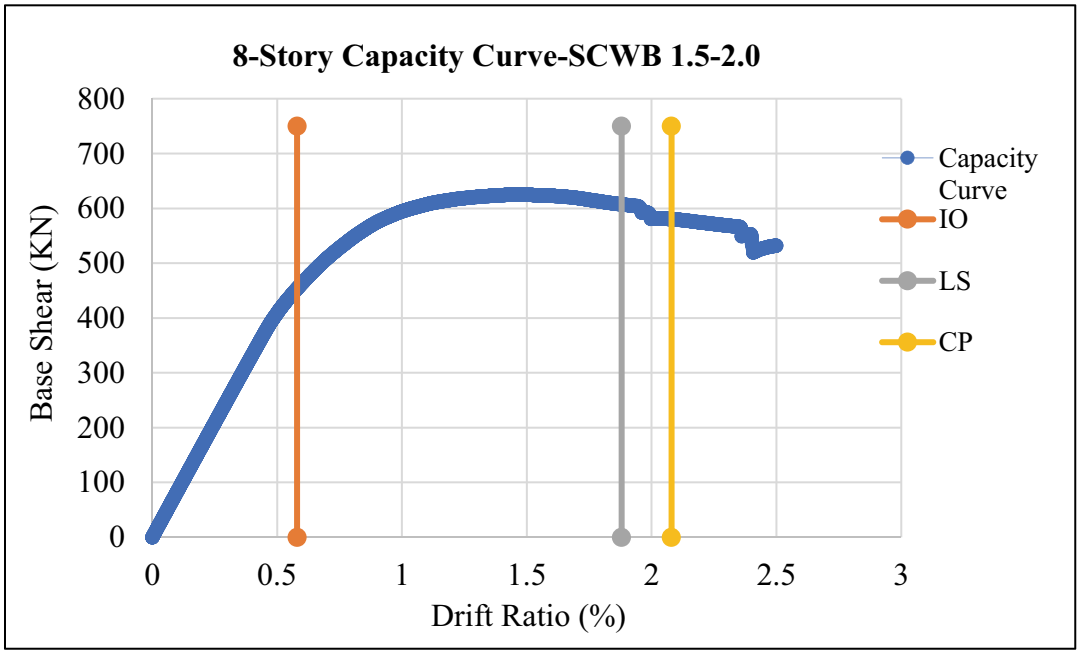

Figure 49. Capacity Curve and Performance Level of the Frame (SCWB: 1.5-2.0)

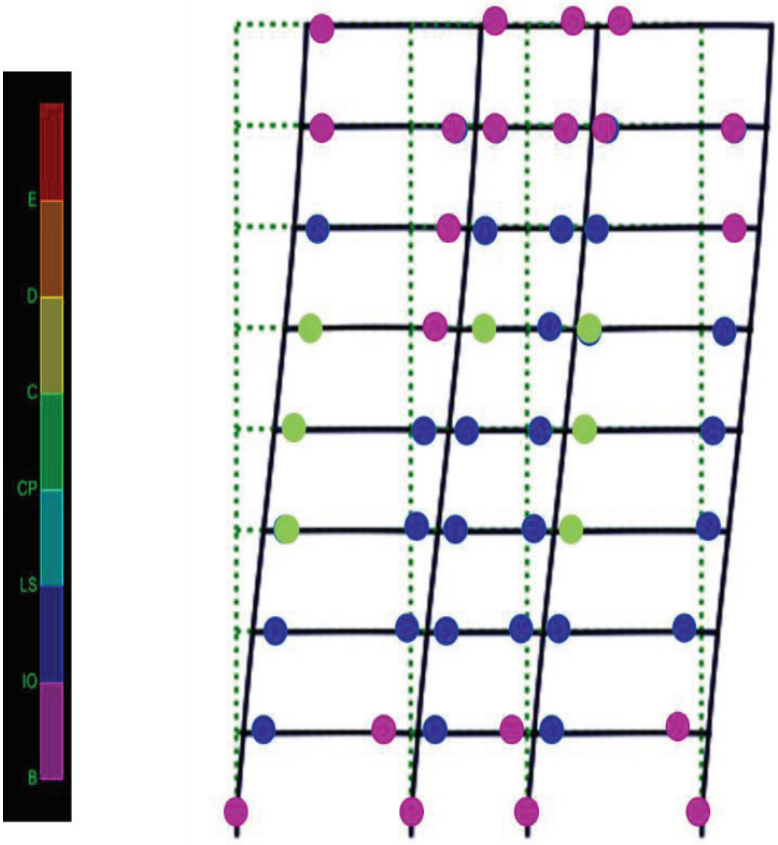

Figure 50. Sway mechanism of the frame obtained from static nonlinear analysis for SCWB of 1.5 up to 2.0

4.4.2.2 Time-History Analyses

Figure 58 displays the scaled-rotation for each hinge as the outcome of the time-history analysis of the frame. The system revealed through time-history analysis that it has almost complete beam hinge mechanism.

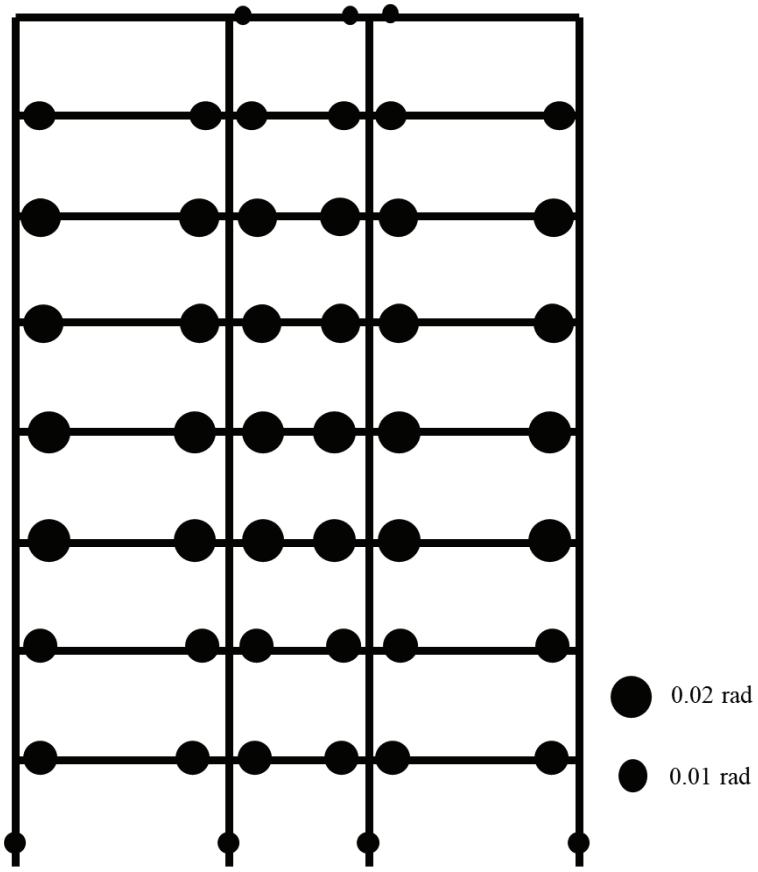

Figure 51. Rotation of each element obtained through time history analysis for SCWB of 1.5-2.0

4.4.3 Eight-Story Three-Bay Frame with SCWB ratio of 2.0-3.0

In this case, the third trial changed the SCWB range to 2.0-3.0. The procedures and other requirements from the previous ones' are still in effect. Information on the reinforcement and cross-sectional details of the system can be found in Tables 25 and 26. The SCWB ratio for each joint is shown in Table 27 for this case. The initial period for this frame is 0.98 sec.

Table 25. Cross sections for internal and external columns with reinforcement details. All dimensions are in mm.

Story	Longitudinal Reinforcement		Transverse Reinforcements				Cross Sectional Size	
	Inner	Outer	Inner		Outer		Inner	Outer
			Confined Region	Unconfined Region	Confined Region	Unconfined Region		
1	12Φ20	12Φ22	Φ8/100	Φ8/130	Φ8/100	Φ8/130	600x600	500x500
2	12Φ20	12Φ22	Φ8/100	Φ8/130	Φ8/100	Φ8/130	600x600	500x500
3	12Φ20	12Φ22	Φ8/100	Φ8/130	Φ8/100	Φ8/130	600x600	500x500
4	12Φ20	12Φ22	Φ8/100	Φ8/130	Φ8/100	Φ8/130	600x600	500x500
5	12Φ20	12Φ22	Φ8/100	Φ8/130	Φ8/100	Φ8/130	600x600	500x500
6	12Φ18	12Φ22	Φ8/100	Φ8/150	Φ8/120	Φ8/150	500x500	500x500
7	12Φ18	12Φ22	Φ8/100	Φ8/150	Φ8/120	Φ8/150	500x500	500x500
8	12Φ18	12Φ22	Φ8/100	Φ8/150	Φ8/120	Φ8/150	500x500	500x500

Table 26. Reinforcement and Cross-sections detail of beams, dimensions are in mm.

Story	Location	Inner Bay	Outer Bay	Cross Sectional Size	
		Support	Support		
Longitudinal Reinforcement				Inner	Outer
1	Top	6Φ20	6Φ20	350x600	
	Bottom	3Φ20	3Φ20		
2	Top	6Φ20	6Φ20		
	Bottom	3Φ20	3Φ20		
3	Top	6Φ20	6Φ20	300x500	350x600
	Bottom	3Φ20	3Φ20		
4	Top	6Φ20	6Φ20		
	Bottom	3Φ20	3Φ20		
5	Top	6Φ20	6Φ20	300x500	
	Bottom	3Φ20	3Φ20		
6	Top	6Φ14	6Φ20		
	Bottom	3Φ14	3Φ20		
7	Top	6Φ14	6Φ20		
	Bottom	3Φ14	3Φ20		
8	Top	6Φ14	6Φ20		
	Bottom	3Φ14	3Φ20		
Transverse Reinforcement					
1	2 legs	Φ10/110	Φ10/110	350x600	
2	2 legs	Φ10/110	Φ10/110		
3	2 legs	Φ10/90	Φ10/90	300x500	
4	2 legs	Φ10/90	Φ10/90		
5	2 legs	Φ10/90	Φ10/90		
6	2 legs	Φ10/90	Φ10/90		
7	2 legs	Φ8/100	Φ8/100		
8	2 legs	Φ8/100	Φ8/100		

Table 27. Column-to beam flexural strength ratios of joints for SCWB 2.0-3.0

Joints	**Column-to-beam strength ratios**
1	4.93(1)
2	2.26
3	2.52
4	2.7(1)
5	4.85(1)
6	2.18
7	2.42
8	2.66(1)
9	4.77(1)
10	2.2
11	2.78
12	2.6(1)
13	4.73(1)
14	2.1
15	2.6
16	2.51(1)
17	4.27(1)
18	2.3
19	2.4
20	2.7(1)
21	3.0(1)
22	2.0
23	2.01
24	1.98(1)
25	2.75(1)
26	2.11
27	2.35
28	1.77(1)
29	1.3(1)
30	1.0(1)
31	1.1(1)
32	0.81(1)

4.4.3.1 Pushover Analyses

Pushover analysis was used to examine the frame in order to check for plastic hinges in the members. A pushover analysis is carried out using the OpenSees platform. The results of the nonlinear static analysis and performance level of frame are shown (See Figure 59). The individual performance level of the hinges is shown in Figure 60.

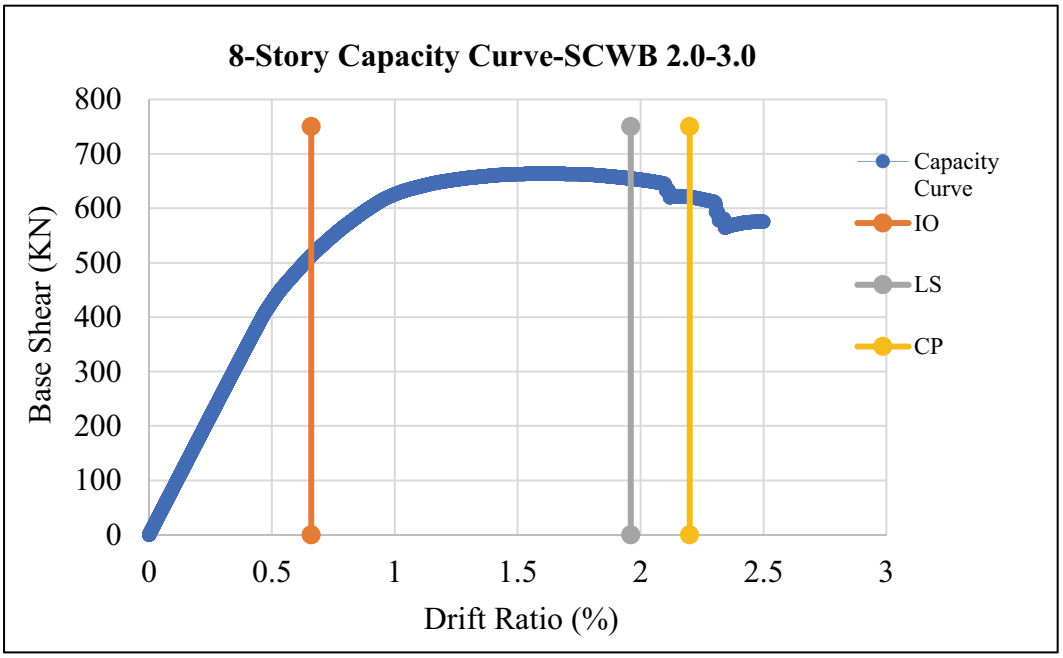

Figure 52. Capacity Curve and Performance Level of the Frame (SCWB: 2.0-3.0)

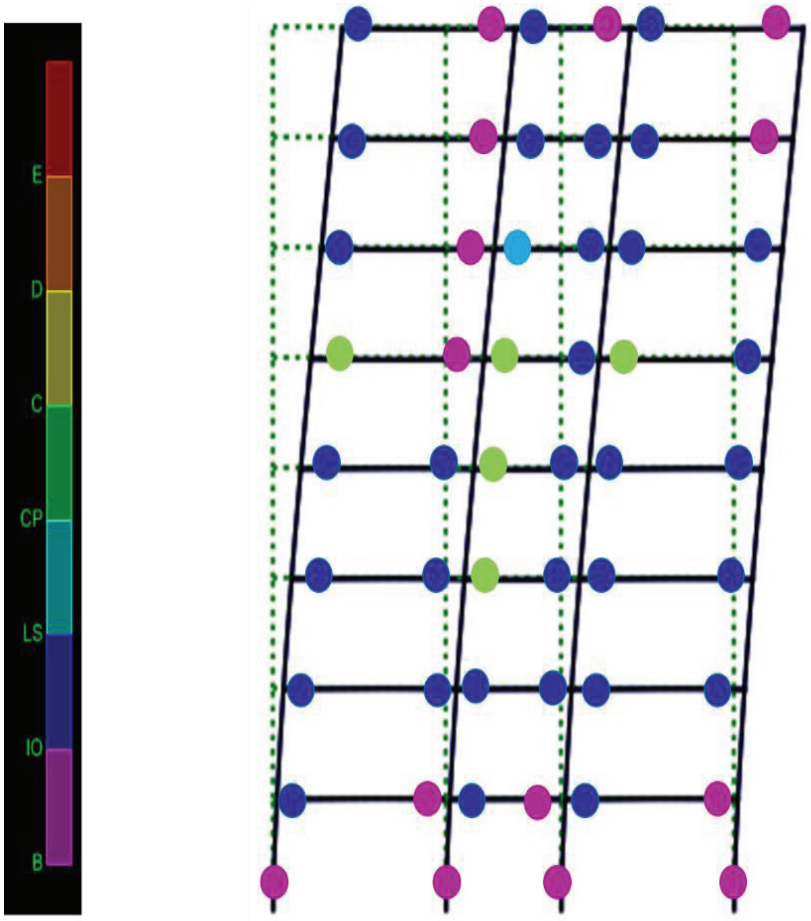

Figure 53. Sway mechanism of the frame obtained from static nonlinear analysis for SCWB of 2.0 up to 3.0

4.4.3.2 Time-History Analyses

Scaled ground motion records were applied to the frame to track the occurrence of plastic hinges in the members. Figure 61 shows that almost full mechanism has been accomplished and the average absolute maximum rotation values in the frame as determined by time-history analysis is also shown. The flexural design ratio for the components is shown in Table 28.

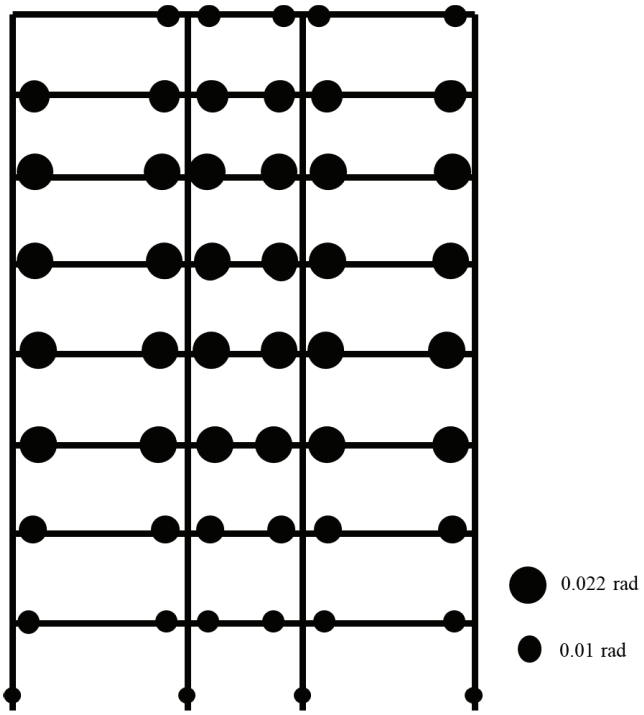

Figure 54. Rotation of each element obtained through time history analysis for SCWB of 2.0-3.0

4.4.4 Discussion of the Results for Eight-Story Three-Bays Frames

The capacity curves and performance levels of all three frames demonstrate a small improvement in the behavior as the SCWB increases. Performance levels such as IO (Immediate Occupancy) improve as the location changes. In addition, compared to the results of early cases, more beams are involved in the failure mechanism as SCWB rises shown in Figure 60. This small improvement can also be seen in Figure 61, where scaled-rotations shows more beams reaching their capacities. It can be also seen that as the SCWB increases, the greatest rotation shifts to higher stories.

CHAPTER 5

SUMMERY AND CONCLUSION

Developing a collapse mechanism that ensures the beams to develop hinges in flexure rather than the columns is one of the most crucial targets in seismic design of moment frame structures. Regulations typically attempts to provide this behavior by strong-column weak-beam strategy. According to the Turkish Earthquake Regulation (TER 2018), the summation of column moment capacities must be at least 20% greater than the summation of beams at a joint. However, some researches have demonstrated that this limit should be increased in order to attain better behavior.

In this study, different range of SCWB (Strong-Column Weak-Beam) ratios has been investigated to see the effect of the change. The studied SCWB ratios are 1.2-1.5, 1.5-2.0, and 2.0-3.0. These ratios are implemented on three reinforced concrete frames types (three-bays two-story, five-story and eight-story 2D). The design procedure dictated by Turkish Earthquake Regulation (TER 2018) is implemented for each frame.

Pushover and time-history analysis were conducted to observe the behavior of the frames. OpenSees software was used to perform pushover analysis. Plastic hinge rotations were followed and used for defining the performance levels of the elements and the overall frames. Time-history analysis are performed for the eleven scaled ground motions that satisfies the TER 2018 requirements.

The performance levels for the immediate occupancy, life safety, and collapse prevention, as defined in TER 2018, are calculated for each frame. The results show minimal difference for two story frames, as shown in Figures 34, 37, and 40. It can be observed how the plastic hinges' formation has been slightly improved and shifted to resemble a beam hinge mechanism from Figures 36, 39, and 42.

The capacity curves and performance levels of all three chosen ranges for five-story three-bays frames demonstrate a small improvement in the behavior as the SCWB rises. Pushover analysis show that there is a slight increase in the distance between IO (Immediate Occupancy) and LS (Life Safety) levels. In addition, compared to the results of early cases, more beams are involved in the failure mechanism as SCWB rises, as

shown in Figure 49. This small improvement can also be seen in Figure 51, where scaled-rotation shows more beams reached their yield capacities.

For eight-story three-bays frames, the performance levels and capacity curves demonstrate a minor change in the behavior as the SCWB increases. As SCWB ratio rises, performance levels such as IO (Immediate Occupancy) improves. More beams are also involved in the failure mechanism as SCWB increases, as shown in Figure 59, compared to the outcomes of early cases. Scaled-rotations in Figure 61 demonstrate this slight increase by revealing more beams achieving their capacities. It can be observed that the greatest rotation moves to higher stories as the SCWB rises.

The relative insensitivity of the collapse mechanisms to the changes in the increase of column to beam strength ratio at the joints could be partially attributed to the mismanagement of design decisions of frames. Unfortunately, an unintentional design decision makes it difficult to follow the effect in changes of SCWB strength ratios. Some of the moment strength ratios of columns to beams at the joint is increased by decreasing the beam flexural capacities. This is a clear indication that at the 1.2-1.5 ratio there was an over-strength in the beams that permits such a strategy. Possibly due to this mismanagement, the frame maximum shear ratios do not change meaningfully or even decrease for some of the frames for higher column to beam strength ratios. It could be discussed that such a decision is acceptable since the moment strength ratio is the main parameter. Obviously, it inserts an another parameter into discussion that possibly blurs the results from a clear conclusion.

This exercise proves that the one should be very careful in selecting and keeping a clear path for having ability to make clear conclusions from a study.

There is one clear conclusion that could be made from the study that keeping the column to strength ratio as the only parameter is not sufficient for observing the relative effects of the changing strength ratio in the frames.

REFERENCES

Ahmad, Shuaib H., and Surendra P. Shah. "Complete triaxial stress-strain curves for concrete." Journal of the Structural Division 108, no. 4 (1982): 728-742.

Allahabadi, Rakesh. Drain-2DX: Seismic Response and Damage Assessment for Two-Dimensional Structures. University of California, Berkeley, 1987.

American Society of Civil Engineers. *Seismic Evaluation and Retrofit of Existing Buildings (ASCE/SEI 41-13)*; 2013.

Berry, Michael P., and Marc O. Eberhard. "Performance modeling strategies for modern reinforced concrete bridge." University of California, Berkeley (2008).

Bouc, R. "Forced vibrations of mechanical systems with hysteresis." In Proc. of the Fourth Conference on Nonlinear Oscillations, Prague, 1967. 1967.

Caterino, N., E. Cosenza, and B. M. Azmoodeh. "Approximate methods to evaluate storey stiffness and interstory drift of RC buildings in seismic area." Structural engineering and mechanics 46, no. 2 (2013): 245-267.

Chang, G. A., and John B. Mander. Seismic energy based fatigue damage analysis of bridge columns: Part I-Evaluation of seismic capacity. Buffalo, NY: National Center for Earthquake Engineering Research, 1994.

Choi, Se Woon, Keunhyoung Park, Byung Kwan Oh, Yousok Kim, and Hyo Seon Park. "Optimal seismic design method to induce the beam-hinging mechanism in reinforced concrete frames." In NCEE 2014-10th US National Conference on Earthquake Engineering: Frontiers of Earthquake Engineering. 2014.

Zaghi, Arash E., Siavash Soroushian, Ahmad Itani, E. Manos Maragakis, Gokhan Pekcan, and Masoud Mehrraoufi. "Impact of column-to-beam strength ratio on the seismic response of steel MRFs." Bulletin of Earthquake Engineering 13 (2015): 635-652.

Ersoy, U., Özcebe, G., and Tankut, T., “Reinforce Concrete.” Middle East Technical University (METU), Ankara Turkey: METU Press. ISBN:978-605-4362-17-2. 2013.

Gharakhanloo, Armin. "Distributed and concentrated inelasticity beam-column elements used in earthquake engineering." Master's thesis, Dissertation, Norwegian University of Science and Technology, Trondheim, Norway, 2014.

Guidelines for Nonlinear Structural Analysis for Design buildings, NIST GCR 17-917-46v1 , 2017

Hachem, Mahmoud Mohamad, Jack P. Moehle, and Stephen A. Mahin. Performance of circular reinforced concrete bridge columns under bidirectional earthquake loading. Berkeley, CA: Pacific Earthquake Engineering Research Center, 2003.

Haselton, Curt B. "Assessing seismic collapse safety of modern reinforced concrete moment frame buildings." PhD diss., Stanford University, 2006.

Ibarra, Luis F., Ricardo A. Medina, and Helmut Krawinkler. "Hysteretic models that incorporate strength and stiffness deterioration." Earthquake engineering & structural dynamics 34, no. 12 (2005): 1489-1511.

Kaklauskas, Gintaris, and Jamshid Ghaboussi. "Stress-strain relations for cracked tensile concrete from RC beam tests." Journal of Structural Engineering 127, no. 1 (2001): 64-73.

Karsan, I. Demir, and James O. Jirsa. "Behavior of concrete under compressive loadings." Journal of the Structural Division 95, no. 12 (1969): 2543-2564.

Kent, Dudley Charles, and Robert Park. "Flexural members with confined concrete." Journal of the structural division 97, no. 7 (1971): 1969-1990.

Lignos, Dimitrios. Sidesway collapse of deteriorating structural systems under seismic excitations. Stanford university, 2008.

Mander, John B., Michael JN Priestley, and R. Park. "Theoretical stress-strain model for confined concrete." Journal of structural engineering 114, no. 8 (1988): 1804-1826.

Mazzoni, Silvia, Frank McKenna, Michael H. Scott, and Gregory L. Fenves. "OpenSees command language manual." Pacific Earthquake Engineering Research (PEER) Center 264, no. 1 (2006): 137-158.

McKenna, Frank, Michael H. Scott, and Gregory L. Fenves. "Nonlinear finite-element analysis software architecture using object composition." Journal of Computing in Civil Engineering 24, no. 1 (2010): 95-107.

Menegotto, Mi, and P. E. Pinto. “Method of analysis for cyclically loaded reinforced concrete frames including changes in geometry and non-elastic behavior of elements under combined normal forces and bending moment.” IASBE Proceedings (1973).

Nakashima, Masayoshi, and Shinichi Sawaizumi. “Column-to-beam strength ratio required for ensuring beam-collapse mechanisms in earthquake responses of steel moment frames.” In Proceedings of the 12th World Conference on Earthquake Engineering, vol. 38, pp. 52-29. New Zealand Society for Earthquake Engineering, 2000.

NIST, Guidelines for Nonlinear Structural Analysis for Design of Buildings, Part I – General, NIST GCR 17-917-46v1, prepared by the Applied Technology Council for the National Institute of Standards and Technology, Gaithersburg, Maryland. 2017.

Nojavan, Alireza, Arturo E. Schultz, Shih-Ho Chao, and Curt B. Haselton. "Influence of cross-sectional size on seismic performance of reinforced concrete columns." ACI Structural Journal 114, no. 2 (2017): 311-321.

Nojavan, Alireza, A. E. Schultz, S. H. Chao, C. Haselton, S. Simasathien, G. Palacios, and X. Liu. "Preliminary results for NEESR full-scale RC column tests under collapse-consistent loading protocols." In 10th US National conference on earthquake engineering, Anchorage, AK. 2014.

Park, Robert, MJ Negel Priestley, and Wayne D. Gill. "Ductility of square-confined concrete columns." Journal of the structural division 108, no. 4 (1982): 929-950.

Paulay, Thomas, and MJ Nigel Priestley. Seismic design of reinforced concrete and masonry buildings. Vol. 768. New York: Wiley, 1992.

Pincheira, JoséA, Faridun S. Dotiwala, and Jonathan T. D'Souza. "Seismic analysis of older reinforced concrete columns." Earthquake Spectra 15, no. 2 (1999): 245-272.

Popovics, Sandor. "A numerical approach to the complete stress-strain curve of concrete." Cement and concrete research 3, no. 5 (1973): 583-599.

Razvi, Salim, and Murat Saatcioglu. "Confinement model for high-strength concrete." Journal of Structural Engineering 125, no. 3 (1999): 281-289.

SAP2000, CSI Analysis Reference Manual For SAP2000®, ETABS®, SAFE® and CSiBridge. CSI Computers & Structures, Inc. Berkeley, California, USA. ISO# GEN062708M1 Rev.11, 2018.

Sudarsana, I. Ketut, Ida Ayu Made Budiwati, and Putu Wiyta Aditya. "Effect of column to beam strength ratio on performance of reinforced concrete frames." (2014).

Takeda, Toshikazu, Mete A. Sozen, and N. Norby Nielsen. "Reinforced concrete response to simulated earthquakes." Journal of the structural division 96, no. 12 (1970): 2557-2573.

TEC2018. Turkish Earthquake Code for Building Structures: Specifications for Design of Buildings under Earthquake Forces; Presidency of Disaster and Emergency Management, 2018.

Torres, Ll, Francisco López-Almansa, and L. M. Bozzo. "Tension-stiffening model for cracked flexural concrete members." Journal of Structural Engineering 130, no. 8 (2004): 1242-1251.

TS500, Requirements for Design and Construction of Reinforced Concrete Structures. English version, publication NO.2003/1. Turkish Standards Institute, Ankara Turkey, 2003.

Wen, Yi-Kwei. "Method for random vibration of hysteretic systems." Journal of the engineering mechanics division 102, no. 2 (1976): 249-263.

Zareian, Farzin. Simplified performance-based earthquake engineering. Stanford University, 2006.

Zhang, Hao, Zhanxuan Zuo, Maosheng Gong, and Lili Xie. "Analysis of the Effect of Column-to-Beam Strength Ratio on Seismic Performance of RC Frame Structure." In IOP Conference Series: Earth and Environmental Science, vol. 304, no. 5, p. 052107. IOP Publishing, 2019.